UHRF2 regulates cell cycle, epigenetics and gene expression to control the timing of retinal progenitor and ganglion cell differentiation

Xiaohong Wang[1], Aaron L. Sarver[2], Qiyuan Han[4], Christopher L. Seiler[4], Chencheng Xie[1], Huarui Lu[1], Colleen L. Forster[3], Natalia Y. Tretyakova[4], Timothy C. Hallstrom[1,5]

[1]Department of Pediatrics, Division of Blood and Marrow Transplantation, 420 Delaware Street S.E., University of Minnesota, Minneapolis, MN 55455, USA.
[2]Institute for Health Informatics, Masonic Cancer Center, University of Minnesota, Minneapolis, MN, 55455, USA
[3]BioNet, Academic Health Center, University of Minnesota, Minneapolis, MN, 55455, USA
[4]Department of Medicinal Chemistry, University of Minnesota, Minneapolis, MN, 55455, USA.

[5]**Corresponding Author:** Timothy C. Hallstrom, 420 Delaware Street S.E., MMC 366, Minneapolis, MN, 55455. Phone: 612-626-2905. halls026@umn.edu

Keywords: UHRF2, retina, development, 5hmC, 5-hydroxymethylcytosine, TET

Summary Statement

UHRF2 promotes retinal progenitor cell G_1 cell cycle arrest, increases 5hmC, and regulates gene expression, favoring progenitor retention over ganglion cell production during retinal development.

Abstract

Ubiquitin like with PHD and ring finger domains 2 (UHRF2) regulates cell cycle and binds 5-hydroxymethylcytosine (5hmC) to promote completion of DNA demethylation. *Uhrf2*$^{-/-}$ mice are without gross phenotypic defects, however the cell-cycle and epigenetic regulatory functions of *Uhrf2* during retinal tissue development is unclear. Retinal progenitor cells (RPCs) produce all retinal neurons and Müller glia in a predictable sequence controlled by the complex interplay between extrinsic signaling, cell cycle, epigenetic changes, and cell-specific transcription factor activation. In this study we find that UHRF2 accumulates in RPCs, and its conditional deletion from RPCs reduced 5hmC, altered gene expressions, and disrupted retinal cell proliferation and differentiation. Retinal ganglion cells were overproduced in *Uhrf2*-deficient retinae at the expense of VSX2^{+} RPCs. Most other cell types were transiently delayed in differentiation. Expression of each member of the *Tet3*/*Uhrf2*/*Tdg* active demethylation pathway was reduced in *Uhrf2*-deficient retinae, consistent with locally reduced 5hmC in their gene bodies. This study highlights a novel role of UHRF2 in controlling the transition from RPCs to differentiated cell by regulating cell cycle, epigenetic and gene expression decisions.

Introduction

Development of the retina involves the highly coordinated generation of six neural and one glial cell type in correct numbers and at the appropriate time from a pool of multipotent retinal progenitor cells (RPCs) (Cepko, 2014, Bassett and Wallace, 2012, Centanin and Wittbrodt, 2014). Retinal ganglion cells (RGCs) are produced first during embryogenesis, followed by cone photoreceptors, horizontal cells, and amacrine neurons (Waid and McLoon, 1995, Mu and Klein, 2004). Rod photoreceptors, Müller glia, and bipolar cells are mostly generated after birth, and cell proliferation is complete by post-natal day 10 (P10) in the mouse retina (Young, 1985). Many extrinsic and intrinsic factors balance the maintenance of RPCs with the production of new cell types by controlling cell cycle exit, interkinetic nuclear migration, and symmetric versus asymmetric cell division (Cepko et al., 1996, Agathocleous and Harris, 2009, Wallace,

2011, Seritrakul and Gross, 2019, Dyer and Cepko, 2001, Baye and Link, 2007, Del Bene et al., 2008). Extrinsic factors adjust and diminish RPC multipotential fate over the developmental window (Austin et al., 1995, Cepko et al., 1996, Xiang, 2013, Aldiri et al., 2017, Wallace, 2011, Bassett and Wallace, 2012). RPC fate is also regulated through highly coordinated changes to key lineage-driving transcription factors and the epigenetic status of their transcriptional target (Cepko, 2014, Brzezinski and Reh, 2015, Kim et al., 2016, Mo et al., 2016, Swaroop et al., 2010, Corso-Díaz et al., 2018, Seritrakul and Gross, 2019, VandenBosch and Reh, 2020).

DNA methylation of cytosine in CpG dinucleotides (5mC) plays a key role in regulating gene expression during retinal development (Mo et al., 2016, Kim et al., 2016, Corso-Díaz et al., 2018, Dvoriantchikova et al., 2019). The methylation status of the genome is maintained during DNA replication by the coordinated activity Ubiquitin like with PHD and ring finger domains 1 (UHRF1) protein and DNA methyltransferase I. UHRF1 binds to newly replicated hemi-methylated DNA strands and recruits DNMT1 protein into proximity to accurately copy the methylation pattern to the daughter strand (Sharif et al., 2007, Bostick et al., 2007, Zhang et al., 2011, Rothbart et al., 2012). A loss of either DNMT1 or UHRF1 can lead to passive DNA demethylation during replication (Liu et al., 2013). Methyl groups can be directly removed through an iterative process not requiring cell division called active demethylation (Tahiliani et al., 2009, Koh and Rao, 2013, Rasmussen and Helin, 2016). This process begins when Ten-eleven translocation (TETs) enzymes oxidize 5-methylcytosine (5mC) to 5-hydroxymethylcytosine (5hmC) (Kriaucionis and Heintz, 2009, Shen and Zhang, 2013, Tahiliani et al., 2009). 5hmC coordinates the expression of genes important for cellular differentiation, and is critical for proper development of the retina and most tissues (Ficz et al., 2011, Hahn et al., 2013, Perera et al., 2015, Seritrakul and Gross, 2017). 5hmC can be further oxidized to 5-formylcytosine (5fC) and 5-carboxylcytosine (5caC) by Tet proteins (Ito et al., 2011) and these bases are enzymatically replaced to cytosine by the thymine DNA glycosylase (TDG) enzyme (He et al., 2011, Weber et al., 2016). TET activity is critical for eye development (Xu et al., 2012) as *tet2* and *tet3* knockdowns reduced 5hmC locally to alter gene expression and impaired retinal tissue development (Seritrakul and Gross, 2017).

UHRF2, a paralog of UHRF1, was identified as an E3-ubiquitin ligase involved in cell cycle regulation (Mori et al., 2002, Mori et al., 2011). Although structurally homologous to UHRF1, ectopic UHRF2 expression cannot replace the methylation defect in *Uhrf1*$^{-/-}$ embryonic stem cells, or compensate for *Uhrf1* deletion in mice suggesting these two proteins possess distinct functions (Zhang et al., 2011, Pichler et al., 2011, Vaughan et al., 2018). UHRF2 was recovered from neural progenitor cells as a 5hmC binding protein (Spruijt et al., 2013). UHRF2 co-localizes with 5hmC in cancer cell lines using chromatin and DNA immunoprecipitation comparisons (Liu et al., 2016). *Uhrf2* germline knock-out mice are viable and exhibit no gross phenotypic defects but show altered neural gene expression and decreased 5mC at specific loci (Chen et al., 2017, Liu et al., 2017). The co-crystal structure of the UHRF2 SET and RING-associated (SRA) domain bound to 5hmC was solved (Zhou et al., 2014). UHRF2 associates with the base-excision repair (BER) complex and can promote TDG-mediated active demethylation (Liu et al., 2021). UHRF2 protein is widely expressed in neural, intestinal and common lymphoid progenitor cells and generally remains expressed in post-mitotic tissues (Spruijt et al., 2013 , Munoz et al., 2012, Lu et al., 2016, Li et al., 2020). However, UHRF2 function has not been investigated in RPCs.

In this publication we show that UHRF2 levels are elevated in RPC-rich whole retinae at P0 compared to differentiated cells. *Uhrf2* deletion from RPCs delayed cell cycle arrest and increased total cell numbers and KI67^{+} proliferating retinal cells. Retinal ganglion cells (RGCs) were overproduced in *Uhrf2*-deficient retinae, partially at the expense of RPCs which were reduced. Other retinal cell types including rod, cone, horizontal, bipolar and Müller Glia retinal cell types exhibited delayed differentiation that were mostly restored by P30. *Uhrf2*-deficiency reduced 5hmC both globally, and locally within the gene bodies of the *Tet3-Uhrf2-TDG* active demethylation circuitry contributing to their reduced expression. In contrast, the rod specific gene Rhodopsin (*Rho*) which undergoes demethylation during rod photoreceptor development, was less methyl- and hydroxymethylated across the promoter and its expression was further induced in *Uhrf2*-deficient retinae. These findings collectively indicate that UHRF2 regulates cell cycle of RPCs and controls 5hmC homeostasis to alter gene expression and augment progenitor differentiation.

RESULTS

UHRF2 is highly expressed in retinal cell progenitor cells (RPCs) and restricts their over-proliferation.

We first examined the expression patterns of *Uhrf2* in the developing and post-natal retina. RNA was isolated from control and *Uhrf2*-deficient retinae at P0 and P30 to determine *Uhrf2* mRNA levels by quantitative PCR (qPCR) using primer sets that span exons 2-3, 7-8 and 15-16 (Fig. 1A). In each case, *Uhrf2* mRNA levels were significantly reduced by around 75% at P30 compared to P0. UHRF2 protein levels were assessed by immunoblotting at P0, P7 and P30 using three independent samples (Fig. 1B). UHRF2 protein levels were quantified and normalized against β–actin loading control and was more abundant at P0 than at P7 and P30 (Fig. 1C). We tested UHRF2 function by conditionally deleting the *Uhrf2* gene from RPCs. Mice with *Uhrf2* exon 3 sequence flanked by *loxP* sites (Fig. 1D) were crossed with mice carrying the visual system homeobox 2 (*Vsx2)* promoter driving expression of a *Cre:Gfp* transgene to generate *Vsx2-Cre*$^{+}$*; Uhrf2*$^{fl/fl}$ offspring (Rowan and Cepko, 2004). The *Vsx2* promoter expresses Cre recombinase in RPCs so all neural and Müller glial retinal cell types are affected by the deletion. We confirmed the loss of *Uhrf2* mRNA by qPCR analysis using primers spanning exons 2 and 3 (Fig. 1E) and UHRF2 protein by immunoblotting (Fig. 1F). Sections from control and knockout retina were cut and stained with hematoxylin & eosin for histological examination (Fig. 1G). *Uhrf2*-deletion led to increased retinal cell layer thickness, which was particularly notable at P7. *Uhrf2*-deletion significantly increased total retinal cell numbers, compared to wild-type retinae, at P0, P3, and P7 but cell numbers were restored to levels observed in control cells by P30 (Fig. 1H).

Uhrf2 **deletion in RPCs causes excess G1/S passage and proliferation.** We detected proliferative cells by immuno-staining wild-type and *Uhrf2*-deficient retinae with anti-KI67 antibodies. *Uhrf2*-deficiency led to increased KI67^{+} cells early and throughout post-natal development (Fig. 2A). KI67^{+} cells were elevated at P0 and P3 throughout the neuroblastic layer (NBL) of *Uhrf2*-deficient retinae. Control retinal cells are almost all post-mitotic at P7, however, KI67^{+} retinal cells are still present in *Uhrf2*-deficient retinae at P7. No proliferating cells were detected at P30 in control or *Uhrf2*-deficient retinae.

KI67$^+$ cells were quantified in P0, P3, P7, and P30 control and *Uhrf2*-deficient retinae and graphed (Fig. 2B). The results demonstrate significant hypercellularity in *Uhrf2*-deficient retina through post-natal development that equilibrates in the mature retina. The retinoblastoma (pRB) cell cycle regulator is phosphorylated by cyclin/CDK phosphorylation during the G_1/S cell cycle transition (Dyson, 2016). We tested whether *Uhrf2* deletion leads to increased serine 780 phosphorylation of pRB, observing a significant increase in pRB-P (S780) in extracts from knockout retinae (Fig. 2C). Retinal cells expressing CRE:GFP$^+$ fusion from *Vsx2* or negative (CRE:GFP$^-$) were isolated from P0 control and *Uhrf2*-deficient retinae and assessed for cell cycle stages by flow cytometry (Fig. 2D). *Uhrf2*-loss significantly reduced the percentage of retinal cells in G_1-phase and increased the numbers of S-phase and G_2/M-phase cells. We assessed apoptosis in the *Uhrf2*-deleted retinae since deregulation of the Rb/E2F pathway is often associated with increased cell death. The numbers of TUNEL$^+$ apoptotic cells were detected in P0 control and *Uhrf2*-deficient retinae by immunofluorescence (IF) staining (Fig. 2E) and were comparable (Fig. 2F). TUNEL$^+$ apoptotic cells were stained by IHC in P0 and P7 mice (Fig. 2G) and quantified and graphed (Fig. 2H). Levels of apoptosis again were the same between genotypes at P0 but dropped in wild-type retinae at P7, with levels in *Uhrf2*-deleted retinae significantly higher than in P7 control cells. Overall, retinal cells lacking *Uhrf2* phosphorylate pRB and fail to undergo timely growth arrest during development leading to excess KI67$^+$ cells.

UHRF2 is required for proper 5hmC accumulation and gene expression in the developing retina.

We determined how 5hmC levels are affected by location in control and *Uhrf2*-deficient developing retinal tissue by IHC. 5hmC staining was comparable at P0, however individual cells with higher levels of 5hmC were identified in the outer NBL of control cells (Fig. 3A, Top, red arrow). 5hmC visibly increased in much of the NBL of P3 and P7 control versus *Uhrf2*-deficient retinae. Each cell in the control retina stained 5hmC$^+$, but in contrast, many *Uhrf2*-deficient retinal cell types were 5hmC$^-$, particularly evident in photoreceptor cells in the ONL. Intriguingly, cells within the abnormally proliferating INL were a mixture of 5hmC$^+$ and 5hmC$^-$ cells. The 5hmC levels were

comparable in cells of the GCL of both retinae at P7. These differences noted at P7 were largely corrected by P30 when control and *Uhrf2*-deficient cells displayed a similar staining pattern (Fig. 3A, Bottom).

We used isotope dilution high performance liquid chromatography (HPLC) - tandem mass spectrometry to accurately quantify 5mC, 5hmC and 5-formylcytosine (5fC) levels during retinal development in control and *Uhrf2*-deficient retinae at P7 (Fig. 3B left). 5mC levels did not differ significantly but 5hmC levels were reduced by ~30% after *Uhrf2*-deletion compared to control. Furthermore, 5fC, a reliable marker of active demethylation, was also significantly reduced in the *Uhrf2*-deleted retina. These findings indicate that UHRF2 is required for 5hmC and 5fC maintenance during retinal development. Long-term effects of *Uhrf2* deletion on epigenetic marks of DNA at 8-months demonstrated 5hmC levels were equal between control and *Uhrf2*-deficient retinae (Fig. 3B right) but 5fC levels were significantly reduced in aged *Uhrf2* deleted retinae indicating a continued failure of active demethylation. DNA dot-blotting was used to qualitatively measure 5hmC levels in control and *Uhrf2*-deleted retinae at P7 (Fig. 3C). Global 5hmC levels were scanned and compared with methylene blue staining of total DNA and were reduced ~40% in *Uhrf2*-deficient retinae compared to control, consistent with mass spectrometry results.

We tested whether other ‘active demethylation’ components are also highly expressed in RPCs similar to *Uhrf2*. Expression of each of the Tet genes (*Tet1*, *Tet2*, *Tet3*) and *Tdg* were significantly reduced at P30 compared to expression levels at P0 (Fig. 3D), indicating that active demethylation pathway components are more highly expressed in proliferating progenitor than in differentiated retinal cells. The reduced levels of 5hmC observed in *Uhrf2*-deficient retinae at P7 could be caused by several factors. One possibility is that reduced expression of Tet genes at P7 contributes to the reduced 5hmC. Indeed, we observed significantly decreased expression of *Tet1*, *Tet2*, *Tet3*, and *Tdg* in *Uhrf2*-deleted retinal cells at P7 compared to control (Fig. 3E left). Because 5hmC levels were restored in *Uhrf2*-deficient retinae by P30, we anticipated that expression levels of the Tet genes would also be restored. As expected, qPCR analysis indicated that *Tet1*, *Tet2*, *Tet3*, and *Tdg* were all returned to comparable levels in control and knockout retinal cells at P30 (Fig. 3E right).

Uhrf2-deficiency leads to gene expression defects relating to E2F/mitotic cell cycle and multiple extrinsic signaling pathways

Further transcriptional differences in *Uhrf2*-deleted retinae at P7 were uncovered using RNA-sequencing. Fragments Per Kilobase of transcript per Million mapped reads (FPKM) values were generated based on the mapped files and used to assess specific gene expression differences. Transcripts displaying standard deviation > 1 were identified, log transformed, mean centered, and displayed using a heatmap (Fig. 3F). Relative transcript expression level is denoted by the color code blue (low) to yellow (high). In total, 54 genes were significantly induced, and expression levels of 275 genes were reduced in the *Uhrf2*-deleted retina. We used Gene Set Enrichment Analysis (GSEA) comparison of control and *Uhrf2*-deficient retinae to give a comprehensive view of the pattern of changes to gene expression (Fig. 3G) (Mootha et al., 2003, Subramanian et al., 2005). “Hallmark” gene sets with a false discovery rate (FDR) lower than 0.25 were displayed. The normalized enrichment scores (NES) allows comparison of gene set analysis results. One set of reduced genes related to E2F targets relating to G_2M, mitosis DNA damage, and apoptosis (Luo et al., 2013, Motnenko et al., 2018, Lu and Hallstrom, 2013). A second set lacked gene expression responsiveness to developmental extrinsic signaling pathways such as TGF-beta, androgen response, Notch, Wnt/β-catenin, and hedgehog. DNA repair and UV response, metabolism, oxidative phosphorylation, and reactive oxygen species gene sets (shaded pink) were induced upon *Uhrf2*-deletion. Overall, the expression studies indicate that UHRF2 is transiently required to maintain normal 5hmC levels and gene expression during retinal development.

Early cells: _Uhrf2_ loss reduces RPCs and overproduces retinal ganglion cells (RGCs) but not cone photoreceptors.

We next examined whether UHRF2 is required for proper retinal cell differentiation by performing IHC using cell-type specific marker antibodies to detect each retinal cell type in control and *Uhrf2*-deficient developing retinae. The number of $Brn3b^+$ RGCs, the first retinal cells formed, were detected with anti-Brn3b antisera by IHC (Fig. 4A, red arrows) and were significantly overproduced in *Uhrf2*-deficient retinae

at P0, P3, and P7 compared to control but restored to comparable numbers at P30 (Fig. 4B). We utilized the *Vsx2-Cre:GFP* transgene to quantify GFP^+ RPC numbers by flow cytometry across a developmental time course in control and *Uhrf2*-deficient retinae (Fig. 4C) (Rowan and Cepko, 2004). We noted significantly fewer GFP^+ cells in *Uhrf2*-deficient retinae at P0, P3 and P7, but at P18 GFP^+ cell numbers were equalized for both genotypes. At P3, *Uhrf2*-deleted retinae contained almost no GFP^+ RPCs, whereas control retinae contained around 35% GFP^+ RPCs. These findings indicates that UHRF2 limits the production of RGCs from RPCs in normal retinae, but RGCs are significantly overproduced and RPCs reduced upon *Uhrf2*-deletion. A list of genes that promote particular retinal cell fate was generated based on representation in high quality lists (Clark et al., 2019, Bassett and Wallace, 2012, Dvoriantchikova et al., 2019, Xiang, 2013). RNA-seq derived gene expression levels were compared between control and *Uhrf2*-deficient retinae and represented as significantly increased (red), significantly decreased (pink), or not significantly altered (gray). For RPC-related genes, one gene (*Pax6*) was induced upon *Uhrf2*-deletion and 5 genes were significantly reduced in the knockout (*Ikzf1*, *Sox9*, *Dll1*, *Notch1*, and *Ccnd1*) (Fig. 4D). In contrast, 4 genes involved in RGC production were induced following *Uhrf2*-deletion (*Eomes*, *Pou4f1*, *Barhl2*, and *Pou4f2*) and two genes were reduced (*Dlx1* and *Dlx2*) (Fig. 4E). Cone cells, detected with anti-cone arrestin antibody, were present but also delayed in production in *Uhrf2*-deficient retinae at P7 compared to control (Fig. 4F, red arrows). Cone cells remained significantly reduced by around 40% in the *Uhrf2*-deficient retinae at P30 (Fig. 4G). Eight cone-specifying genes were reduced with none induced (Fig. 4H). These data indicate that *Uhrf2* controls proper levels of the early produced RGC, RPC, and cone cells; these changes correlate with altered expression of their related cell-fate driving transcription factors.

Late cells: *Uhrf2*-deficiency causes rod cell mislocalization, rhodoposin overproduction, and delayed bipolar cell production. Rod photoreceptor cells were detected by IHC with anti-rhodopsin antibody. Rod production was strikingly delayed in the *Uhrf2*-deficient retina at P3 (Fig. 5A). By P7, many $rhodopsin^+$ cells had abnormally traversed the outer plexiform layer (OPL) and penetrated the inner nuclear layer (INL)

(Fig. 5A, mid, red arrows). Rhodopsin$^+$ cells mislocalized to the INL were still detected in mature P30 *Uhrf2*-deficient retina (Fig. 5A, bottom, red arrows), and P414 aged retinae (Fig. S1). *Rho*$^+$ cells were quantified in control and *Uhrf2*-deficient retinae and were significantly fewer in knockout retinae at P3 and P7 but levels were equal at P30 (Fig. 5B). Expression of genes that promote rod cell generation was also affected, with *Rho* significantly overproduced in *Uhrf2*-deficient retinae, but the expression levels of six other rod genes were reduced in the knockout (Fig. 5C). These data indicate that UHRF2 controls *Rho* and other rod-specific gene expression, rod cell positioning and production in the developing retina.

We detected bipolar cells in control cells using anti-PKCα (Fig. 5D), and anti-VSX2 antibodies (Fig. 5F), and defects were noted with each in P7 *Uhrf2*-deficient retinae. The numbers of PKCα$^+$ cells were significantly fewer in *Uhrf2*-deleted retinae at P7 compared to control, but by P30 the levels were comparable between genotypes (Fig. 5E). VSX2$^+$ cells were detected as expected in P7 control retinae. VSX2$^+$ cell position was shifted abnormally to the center of the INL closer to the GCL in the knockout retina (Fig. 5F), potentially displaced by the rhodopsin$^+$ cells abnormally located on the incorrect side of the outer plexiform layer (OPL) (Fig. 5A, mid). At P30, the numbers of VSX2$^+$ cells appeared comparable between control and *Uhrf2*-deficient retinae. Bipolar-related gene expression indicates that one gene was induced in the knockout (*Bhlhe23*) and three (*NeuroD1*, *NeuroD4*, and *Ascl1*) were significantly reduced (Fig. 5G). These findings indicate that *Uhrf2*-deficiency contributes to a delay, but not failure, of bipolar cell development.

Uhrf2-deficiency in retinae delays horizontal and Müller glial cell differentiation without affecting amacrine cell production.

Horizontal cells were detected with anti-calbindin antibody in control retinae at P7. Their development was delayed in *Uhrf2*-deficient retinae (Fig. 6A, red arrows) but were comparable to control retinae at P30. The expression levels of five of seven horizontal cell genes queried was reduced at P7 in knockout cells compared to control (Fig. 6B). *Uhrf2*-deficiency also affected gliogenesis, as Müller glia and axon connections were not detected in the knockout retinae at P7 by IHC using anti-CRALBP

antibody (Fig. 6C) but were present in both control and *Uhrf2*-deficient P30 retinae. Genes related to Müller glia production were mostly unaffected in the *Uhrf2*-deficient retina, with only *Hey2* showing reduced expression (Fig. 6D). Syntaxin^{+} amacrine cell staining was comparable between control and *Uhrf2*-deficient retinae at P7 and P30 (Fig. 6E). One amacrine promoting gene was induced (*Neurod2*) and three (*Foxn4*, *Neurod1*, and *Neurod4*) were reduced (Fig. 6F). In summary, *Uhrf2*-deficiency led to delays and for some cells long-term defects in production of both neural and glial retinal cell types. However, compensatory mechanisms allow most cells to develop normally after their initial delay in cellular production.

UHRF2 regulates 5mC and 5hmC in target promoters and gene bodies

UHRF2 supports the completion of active demethylation in embryonic stem cells, where *Uhrf2*$^{-/-}$ leads to 5mC accumulation at promoters bound and regulated by UHRF2 (Liu et al., 2021). We chose four target genes for further analysis to elucidate how *Uhrf2* regulates their levels of 5mC, 5hmC, and gene expression in the developing retina. *Tet3*, *Uhrf2*, and *Tdg* comprise the “active demethylation” pathway which facilitates the enzymatic replacement of 5mC marks back to cytosine. *Rho* is an important rod gene that undergoes active demethylation in rod photoreceptors during retinal development to support rod-specific expression (Kim et al., 2016, Dvoriantchikova et al., 2019). The *Rho* gene was significantly induced in *Uhrf2*-deficient retinae by RNA-seq, whereas *Tet3*, *Uhrf2,* and *Tdg* expression were each significantly reduced (Fig. 7A). In order to determine how *Uhrf2* loss could affect the expression of these genes, we employed two techniques to map 5hmC marks in the gene bodies, or 5mC and 5hmC in the CpG islands (CGIs).

Elevated 5hmC within gene bodies outperforms 5mC as a strong predictor of positive gene expression (He et al., 2021). We used 5hmC-DNA-immunoprecipitation followed by quantitative PCR (hMeDIP-qPCR) to explore the *Tet3*, *Tdg*, and *Uhrf2* gene bodies for 5hmC accumulation during retinal development. *Rho* was not analyzed using this assay because it did not accumulate 5hmC in its gene body in this same study (Perera et al., 2015). 5hmC marks were significantly reduced in the gene bodies of *Tet3*, *Tdg*, and *Uhrf 2* (Fig. 7B). Although it is not clear by what mechanism the

presence of 5hmC in the gene body augments gene expression or how UHRF2 stabilizes it, *Uhrf2*-dependent reduction in gene bodies could contribute to decreased levels of gene expression (He et al., 2021). Furthermore, UHRF2 is prominently detected at introns by chromatin immunoprecipitation (Liu et al., 2021).

Simultaneous targeted methylation sequencing (sTM-Seq) reveals distinct effects at different CpGs

Next, we assessed the methylation and hydroxymethylation status of the CGIs located in these genes. We used simultaneous targeted methylation sequencing (sTM-Seq) to generate base resolution detection of 5mC and 5hmC sequences in discrete regions of the mouse *Rho*, *Tet3*, *Tdg*, and *Uhrf2* genes. This approach allows for examination of multiple targeted genes at once. DNA is bisulfite (BS) converted to detect the combined levels of 5mC and 5hmC. A diagram showing the genes and primer locations is shown in Figure S2. *Rho*, a rod-specific phototransduction gene, is highly methylated and poorly expressed in RPCs. As RPCs differentiate into rod cells, the Rho gene undergoes active demethylation and its expression levels rise (Kim et al., 2016, Dvoriantchikova et al., 2019). In non-rod cells however, *Rho* stays methylated and is repressed. Analysis of the *Rho* CGI by sTM-Seq revealed that the *Rho* gene contains less 5mC and 5hmC at 7 of 8 CpGs tested in *Uhrf2*-deficient (yellow) compared to wild-type (blue) retina (Fig. 7C). Oxidative bisulfite (OxBS) “converts” away 5hmC before BS treatment and this allows detection of the remaining 5mC only. 5mC levels were reduced at positions #6 and #8 in *Uhrf2*-deficient (purple) compared to wild-type (green) retina. 5hmC levels were calculated by subtracting the difference between the bisulfite (5mC + 5hmC) and OxBS (5mC). 5hmC levels were significantly reduced at positions #4, #5, and #8. *Uhrf2* loss thus may have distinct effects at different CpGs in terms of maintaining cytosine methylation and hydroxymethylation. Analysis of the *Tet3*, *Uhrf2*, and *Tdg* genes did not reveal significant changes to 5mC or 5hmC in the CGI region analyzed by sTM-Seq (Figure S3). Overall, these data indicate that UHRF2 maintains 5mC and/or 5hmC at specific CpGs in the promoter of *Rho* and this affects *Rho* expression in the knockout. UHRF2 also augments gene expression of members of

the active demethylation pathway by mediating 5hmC accumulation in their gene bodies.

DISCUSSION

Uhrf2-deficiency from RPCs causes RGC overproduction at the expense of RPC maintenance and cone production and delays differentiation of most other retinal neural cell types

In this study we demonstrate that UHRF2 regulates cell cycle and pRB phosphorylation during G_1 phase, controls site-specific methylation and hydroxymethylation at individual CpGs, and changes expression of cell cycle, signaling pathways, and DNA repair genes during retinal development (Fig. 8A). Deleting *Uhrf2* from RPCs caused their premature reduction, overexpression of several key RGC-promoting transcription factors and increased $Brn3b^+$ cell numbers ion the RGC layer. In contrast, there was a decreased number of cone cells, the next differentiating cell type. Most other retinal cell types exhibited delayed differentiation that was later restored, with rod and bipolar cells occasionally positioned improperly (Fig. 8B). These data demonstrate that UHRF2 possesses a role to promote the transition from retinal progenitor to differentiated cells. UHRF2-dependent changes to retinogenesis could be caused by alterations to cell cycle arrest or progression, by changes to the underlying epigenetic status of a cell, or a combination of both.

Uhrf2-deficiency from RPCs increases progenitor cell proliferation by affecting G_1 phase

Here, we show that deleting *Uhrf2* from the retina reduced the percentage of cells in G_1 phase (Fig. 2B) concomitant with phosphorylation of pRB (Fig. 2C). Retinoblastoma (pRB is a critical cell-cycle protein that regulates cell fate during the G_1 phase for cells to permanently exit the cell cycle, growth arrest and differentiate (Weinberg, 1995, Nevins, 1998, Dyson, 2016, Zhang et al., 2004). UHRF2 physically associates with pRB as demonstrated both by direct co-immunoprecipitation (Mori et al., 2011) and by unbiased immunoprecipitation of UHRF2 followed by mass spectrometry identifying pRB among the bound proteins (Lai et al., 2016). UHRF2 was first characterized as a cell cycle

regulatory protein that induced G_1 arrest by ubiquitinating and degrading the pRB-targeting G_1 cyclins D1 and E1, thereby inhibiting cells from undergoing G_1/S passage (Mori et al., 2002, Li et al., 2004). UHRF2 also physically associates with E2F1, a pRB-binding transcription factor, and this can positively regulate expression of the key G_1/S promoting cyclin *Ccne1* (Lu and Hallstrom, 2013). Deletion of *Uhrf2 in vivo* in the retina caused excess $Ki67^+$ cell numbers so it might be expected to see increased E2F activity by GSEA. But instead we observed reduced E2F activity and these genes seem specifically related to G_2M and mitotic spindle targets (Fig.3G). *Uhrf2*-deletion also caused reductions in *Ccnd1* (Fig. 4D) and *Rb1* (Fig. 5C) mRNA by RNA-seq. Relatively few total cells were proliferating in the knockout compared to the total number of cells assayed at P7, and proliferation could have ceased before Ki67 expression was extinguished. Further, it is unclear if the Ser780 pRB-P antibody is detecting mono-phosphoryation of pRB at that site or if Ser780 is one of the many sites included among pRB hyperphosphorylation which is linked to S-phase entry and proliferation. In contrast, deleting *Dnmt1* using the same *Vsx2-Cre* line increased the numbers of cells in G_1 and reduced cells in S/G_2/M (Rhee et al., 2012). DNMT1, UHRF1 and UHRF2 each can physically associate with pRB, and the E3-ubiquitin ligase activity of both UHRF1 & UHRF2 can situationally induce the degradation of DNMTs and cyclins. This suggests a potentially complex interplay between these cell cycle phase regulators during G_1 phase passage (Robertson et al., 2000, Jeanblanc et al., 2005, Jia et al., 2016, Bronner et al., 2007). The overall effects of *Uhrf2*-deletion on G_1 phase progression may pertain to the transition from early- to late-G_1 phase, particularly when considering the reduced gene expression patterns to several G_1 regulating signaling pathways such as Notch and Wnt.

Uhrf2 deletion from RPCs reduces expression of E2F-cell cycle, extrinsic signaling pathways, and DNA repair genes during mouse retinal development

DNA methylation and demethylation play a major role in controlling gene expression and cell fate during retina tissue development (Nasonkin et al., 2013, Corso-Díaz et al., 2018). Other epigenetic regulators, like UHRF2, are expressed in RPCs and exert precise control over DNA methylation and cell fate during retinal development

(Nasonkin et al., 2011, Rhee et al., 2012, Seritrakul and Gross, 2014, Singh et al., 2017, Perera et al., 2015, Seritrakul and Gross, 2017, Seritrakul and Gross, 2019, Corso-Díaz et al., 2018). Zebrafish retinae lacking *dnmt1*, for example, don't maintain adult retinal stem cells (Angileri and Gross, 2020). Although *Uhrf1* has not yet been deleted from RPCs, *Uhrf1* conditional deletion from neural stem cells causes global DNA hypomethylation, premature expression of cell cycle inhibitors and differentiation promoting genes, and stem cell exhaustion (Ramesh et al., 2016, Blanchart et al., 2018). UHRF2 was isolated specifically from neural progenitor cell extracts but not ESCs or mature brain as a 5hmC-binding protein, unlike its counterpart UHRF1 which was recovered from ESCs (Spruijt et al., 2013). UHRF2 is highly expressed in different progenitor cell types, and unlike UHRF1 and although an E2F target gene, it remains expressed in differentiated neural and hematopoietic tissues (Pichler et al., 2011, Spruijt et al., 2013 , Lu et al., 2016, Munoz et al., 2012, Li et al., 2020). Therefore, the roles of UHRF proteins are likely dependent on the developmental status of retinal cells.

In this study we show that *Tet3* and *Tdg* are also more highly expressed with *Uhrf2* in RPC-rich proliferating murine retina (P0) than in mature post-mitotic retinal cells, similar to observations in other progenitor cells (Xu et al., 2012, Hon et al., 2014, Rasmussen and Helin, 2016, Seritrakul and Gross, 2017, Onodera et al., 2021). In the case of *tet2*$^{-/-}$/*tet3*$^{-/-}$ mutant zebrafish, RGCs are specified but then fail to fully differentiate. Photoreceptor cell development was compromised in *tet2* and *tet3* knockouts in zebrafish, which suggested that TET activity mediates active demethylation in these cells during development (Seritrakul and Gross, 2017). This is particularly intriguing because the retinae of *tet2*$^{-/-}$/*tet3*$^{-/-}$ mutant zebrafish also displayed unusually high proliferative rates and also were shown to over-activate Notch and Wnt signaling. Notch and Wnt affect the timing of cell cycle exit and differentiation of progenitors into RGCs (Waid and McLoon, 1995, Austin et al., 1995, Silva et al., 2003). RPCs change their sensitivity to specific extrinsic signals over the developmental time-course (Cepko et al., 1996, Livesey and Cepko, 2001, Dyer and Cepko, 2001, Ohnuma and Harris, 2003). In our study, *Uhrf2*-deficiency led to gene expression defects of several extrinsic signaling pathways critical to retinal development, such as TGF-beta, Notch, Wnt, and sonic hedgehog (SHH), suggesting that UHRF2 may respond to and

regulate these signals to control proliferation, gene expression or cell fate (Fig. 3G). Inhibition of Notch signaling by *Uhrf2*-deletion could contribute to the observed loss of RPC cells (Fig. 4E), which may be more susceptible to increased levels of RGC-promoting transcription factors (Fig. 4G). SHH production by RGCs auto-inhibit further production of RGCs, suggesting that reduced SHH in *Uhrf2*-deficient retinae could conceivably contribute to excess RGC production (Wang et al., 2005). These findings suggest that although TET proteins and UHRF2 are both capable of augmenting 5hmC levels *in vivo*, they may have differential effects on retinal cell fate.

Effects of UHRF2 and other epigenetic regulators on cell fate and gene expression of the *Rho* gene

Photoreceptor specific genes such as *Rho* (rhodopsin), *Gnat1*, and *Cnga1* are methylated with low expression in RPCs and RGCs, but are demethylated and expressed in rod cells where required (Merbs et al., 2012, Kim et al., 2016, Dvoriantchikova et al., 2019). Methylation of the *Rho* CGI is compromised in *Dnmt1* conditional knockout retina (Rhee et al., 2012), and compound disruption of *Dnmt1*, *Dnmt3a*, and *Dnmt3b* activity in mouse retina causes severe hypomethylation of *Rho*, along with defects in photoreceptor differentiation and outer plexiform layer structure (Singh et al., 2017). Genome-wide methylation analysis of DNA derived from purified rod and cone cells indicated that their cell specific gene expression was associated with reduced methylation at the promoter and gene bodies of those targets (Mo et al., 2016). In the retina, *Rho* expression is elevated in mice at post-natal week 3, however 5hmC did not detectably accumulate within *Rho* during this developmental time-frame (Perera et al., 2015). *Uhrf2* deletion in the retina had two primary effects on detection of *Rho*. *Rho* expression was significantly induced in *Uhrf2*-deficient retina (Fig. 7A). Consistent with this observation, combined levels of 5mC and 5hmC were reduced across seven of eight tested *Rho* CpGs. These changes most typically were due to reduced 5hmC without 5mC being affected. Second, the number of RHO^{+} cells detectable by IHC in *Uhrf2* cKO is reduced compared to wild-type at P7. Further analysis is required to understand the mechanisms behind the unusual *Uhrf2*-related changes to *Rho* regulation in the retina.

UHRF2 was recently identified as a key participant with TET and TDG in the active demethylation pathway. 5hmC-binding by UHRF2 coordinates an allosteric change within the protein causing its direct ubiquitinylation of XRCC1, which leads to incorporation of TDG into the base excision repair complex. *Uhrf2* ablation from ESCs was associated with reduced neural progenitor cell differentiation into mature neurons in induction studies (Liu et al., 2021). This defect was associated with site-specific accumulation of 5mC at UHRF2 bound promoters, owing to a failure to complete active demethylation (Liu et al., 2021). In another study, *Uhrf2*$^{-/-}$ germline knock-out mice in contrast decreased 5mC at specific loci, affecting neural gene expression (Chen et al., 2017, Liu et al., 2017, Chen et al., 2018). These and our findings indicate that UHRF2 function may have different effects on CpGs under different times or contexts. It is unclear why some 5hmC marks remains protected from further oxidation and others accumulate over time, particularly in neural tissue, while other sites undergo active demethylation to cytosine (Bachman et al., 2014, Hahn et al., 2014). Individual CpG sites can be differentially regulated and each can have distinct effects on gene expression and cell fate. This was observed for the T-regulatory cell specifying *Foxp3* gene which is dynamically regulated at different CpGs during differentiation (Yue et al., 2016). However, elimination of active demethylation by conditionally deleting *Tdg* from hematopoietic stem cells did not compromise gross hematopoietic development (Onodera et al., 2021). Thus it remains to be deduced how much of UHRF2 activity and role in retinal development depends on active demethylation. Genes besides *Rho*, such as *Tet3, Uhrf2,* and *Tdg,* displayed different regulation and did not undergo significant changes to methylation or hydroxymethylation in their promoters. Instead, during retinal development these genes accumulated 5hmC marks in gene bodies, which is positively correlated with gene expression, and 5hmC levels were reduced at these positions in *Uhrf2*-deficient retinal cells. Future work may involve determining if UHRF2 links histone or DNA epigenetic information to E3-dependent changes in associated proteins that may play a role in 5hmC homeostasis, gene expression, cell cycle or fate.

Materials & Methods

Statistics

Sample sizes were estimated based on power analysis to produce significant outcomes ($p < 0.05$) with 30% differences. No animals or samples were excluded from analysis. IHC and IF staining was performed blinded to animal genotype. P-values were determined by two-tailed Student's *t*-test with $p < 0.05$ considered significant. Error bars represent standard deviation from the mean.

Experimental animals

Vsx2-Cre:GFP Mus musculus (mouse) (Rowan and Cepko, 2004) and related PCR genotyping protocols have been described (Filtz et al., 2015, Xie et al., 2015). Mice with conditional deletion of *Uhrf2* exon 3 in a C57BL/6 background were obtained from The Canadian Mouse Mutant Repository at The Hospital for Sick Children, Toronto. *Vsx2-Cre* and $Uhrf2^{fl/fl}$ mice were bred together to generate $Vsx2\text{-}Cre^{+}; Uhrf2^{fl/fl}$ offspring. Male and female mice were used for experiments. Strain and ages of animals are listed in the figure legends. All mouse experiments were performed in accordance with University of Minnesota Institutional Animal Care and Use Committee procedures and guidelines.

RNA-Sequencing (RNA-Seq) and quantitative PCR (qPCR)

RNA was isolated from retinal tissue using RNeasy Mini Kit (Qiagen), after tissue disruption and homogenization with needles. RNA concentration was calculated using NanoDrop™ 2000/2000c Spectrophotometers (Thermo Scientific™). Libraries were prepared from ~500 ng total RNA with the TruSeq Stranded Total RNA Library Prep Kit according to the manufacturer's directions (Illumina). Paired-end 60 cycle sequencing was performed on HiSeq 2500 sequencers according to the manufacturer's directions (Illumina). Mapping was performed as previously described (Sarver et al., 2021). RT-qPCR was performed using StepOne Real-Time PCR system (Applied biosystems). QuantiTect SYBR Green RT-PCR Kit following manufacture's instruction (Qiagen, Cat.# 204245). We included primer sequences for all qPCR in Table S1. qPCR primer design

and testing was performed according to MIQE guidelines (Bustin et al., 2009, Bustin and Wittwer, 2017).

Immunofluorescence (IF) and immunohistochemistry (IHC)

For IF staining, mouse eyes were embedded in Tissue-Tek OCT compound (Fisher Scientific International, Hampton, NH) and frozen in liquid nitrogen-cooled isopentane. 8 µm thick frozen tissue sections were sectioned on a cryostat and mounted on aminopropyltriethoxysilane-coated slides. The slides were fixed in cold acetone, incubated in 10% normal serum for 30 min before adding in the primary antibody. Visualization was achieved using conjugated secondary antibodies and nuclear staining with 4,6-diamidino-2-phenylindol (DAPI). H&E staining, KI67, TUNEL, and retinal marker IHC staining were performed by the BIONET shared resource as previously described (Xie et al., 2017). Briefly, tissue samples were fixed in 10% formalin and embedded in paraffin. The list of antibodies used is shown in Table S2. Biotinylated secondary antibody, diluted in TBST (20 mM Tris-HCl, pH 7.6; 150 mM NaCl, 0.01% Tween-20) per manufacturer's recommendation, was added to each section and incubated for 30 minutes at room temperature. The slide sections were developed using Vectastain ABC Kits (HRP) or Vectastain ABC-AP Kits (AP) following the manufacture's instruction. The ApopTag Peroxidase kit (EMD Millipore, S7100) was used for TUNEL IHC analysis. Cell numbers were quantified by counting five fields from three independently isolated fixed and stained retinae and are graphed as per cent cells compared to total retinal cells unless specified otherwise.

Cell cycle analysis

Retinal tissue was dissected from mouse eyes and dissociated with trypsin. After digestion, trypsin inhibitor was added and the cell suspension was filtered and pelleted. The cells pellets were fixed in cold 70% ethanol for 1 hour at 4°C, propidium iodide and RNAse A were added and cells were filtered for analysis. Cell cycle data were obtained by FACSCanto (BD Biosciences) and analyzed with FlowJo_V10 software. The retinal cells from *Vsx2-Cre* negative mice (EGFP$^-$), retinal cells from *Vsx2-Cre* positive mice

(EGFP$^+$) and PI staining positive retinal cells were used for gating at the University of Minnesota Flow Cytometry Resource.

Immunoblotting

Immunoblotting was performed as described (Lu et al., 2011, Lu and Hallstrom, 2012). Briefly, mouse retinal tissue was lysed in protein lysis buffer (50mM Tris, pH7.4, 300mM NaCl, 5mM EDTA, 0.5% Nonidet P-40, 50 mM NaF,1 mM Na_3VO_4,1 mM DTT, 1x Sigma protease inhibitor cocktail tablet) for 1 hour. Protein concentration was measured using BCA Protein Assay Kit (Pierce). Equivalent amounts of protein were separated by SDS-PAGE, transferred to PVDF membrane (Millipore), and blocked in TBST (20 mM Tris-HCl, pH 7.6; 150 mM NaCl, 0.01% Tween-20) containing 5% nonfat dry milk. The list of antibodies used is shown in Table S2. Blots were then incubated with primary antibody (1:2000) overnight at 4°C, washed three times with TBST buffer, and then incubated with the appropriate secondary antibody (1:2000) for 1 hour at room temperature. Blots were processed using the ECL system (Amersham Biosciences). The membranes were stripped and reprobed with β-actin antibody to verify equal loading.

Genomic DNA isolation and 5hmC analysis

Genomic DNA was isolated from cells with a QIAamp DNA kit (Qiagen) using RNaseA to eliminate RNA. DNA was diluted at different specified concentrations and dot blotted onto a nitrocellulose membrane and cross-linked using an ultraviolet Stratalinker 1800 (Stratagene). The DNA-immobilized membrane was immunoblotted with rabbit anti-5hmC polyclonal antibody (Active motif, Cat.# 39791). Afterwards, total DNA was stained with 0.04% methylene blue in 0.5M sodium acetate (pH 5.2) over-night, then scanned and quantified against 5hmC.

Capillary HPLC electrospray ionization (ESI) tandem mass spectrometry (HPLC-ESI-MS/MS), and Analytical Methodology for 5mC, 5hmC, and 5fC.

Genomic DNA was extracted from tissues and (1.5 µg) hydrolyzed with phosphodiesterases, DNAse I, and alkaline phosphatase. Samples were spiked with internal standard for mass spectrometry, filtered, and 5fC converted to biotinyl-fC and

enriched using offline HPLC on an Atlantis T3 column and eluted with a gradient of 5 mM ammonium formate and methanol. dC was quantified by HPLC-UV during the HPLC cleanup using calibration curves to normalize the amounts of epigenetic modifications. HPLC fractions corresponding to 5hmC, 5mC, and Biotinyl-fC were combined and analyzed by capillary HPLC-ESI-MS/MS on a Thermo TSQ Vantage mass spectrometer interfaced with a Thermo Dionex Ultimate3000 HPLC. Quantification was conducted in the SRM mode by monitoring the transitions *m/z* 242 → 126 for 5mC, *m/z* 254 → 133 for 5mC standard, *m/z* 258 → 142 for 5hmC, *m/z* 261 → 145 for 5hmC standard, *m/z* 569 → 453 for Biotinyl-fC, and 581 → 460 for Biotinyl-fC standard. Chromatographic separation will be achieved on a Zorbax SB-C18 column eluted at a flow rate of 15 μL/min with a gradient of 2 mM ammonium formate and methanol. The mass spectrometer was operated in negative mode and the parameters for ionization and fragmentation were optimized using authentic standards. Note that % of dC values for both hmC and fC must be multiplied by (10-1) and (10-3) respectively due to their lower abundance. Values are presented as the percent base compared to total cytosine.

5hmC-DNA immunoprecipitation followed by quantitative PCR (hMeDIP-qPCR)

Retinal genomic DNA was sonicated and fragmented to between 100-400 base pair average size. hMeDIP-qPCR was performed following the manufacturer instructions (Active Motif, #55010) with minor modifications. The eluted DNA was treated with proteinase K to remove the immunoprecipitating antibody and then was purified with MinElute PCR purification kit (Qiagen, #28004). The purified DNA was used to perform quantitative PCR. The qPCR reactions were done using the QuantiTect SYBR Green PCR Kit (Qiagen, #204145) in triplicate. Ct value was analyzed to calculate enrichment using the $2^{-\Delta\Delta Ct}$ method (Livak and Schmittgen, 2001). Primer locations for hMeDIP-qPCR were selected by locating 5hmC peaks using Integrative Genomics Viewer on a hMeDIP-Seq dataset generated from mature retinae and are shown in Figure S2 (Perera et al., 2015).

Simultaneous target methylation sequencing (sTM-seq)

Sample preparation and sequencing: Genomic DNA from 3 control (*Vsx2-Cre:GFP*) and 3 experimental (*Vsx2-Cre*$^{+}$*; Uhrf2*$^{fl/fl}$) samples were isolated following the published protocol (Asmus et al., 2019). 5 µg genomic DNA from each sample was spiked with 150 ng standard 5hmC control DNA (Zymo, D5405, Irvine, CA) which was used to assess bisulfite and oxidative bisulfite conversion rates (Fig. S3). The DNA was sonicated (Covaris S220) using the following parameters: Sample volume, 130 µl; Target BP (peak), 500; Peak incident power (w), 105; Duty factor, 5%; Cycles per Burst, 200; Treatment time (s), 80. Followed by DNA sonication, bisulfite and oxBS treatment were performed using the TrueMethyl oxBS-Seq module from Tecan per their instructions but increased the starting material to 1µg. The sTM-seq library construction were modified from a published protocol. Briefly, three PCR steps were used to construct a sTM-Seq sequencing library. The first PCR reactions were run as separate samples to amplify the target regions from the genomic DNA. The PCR products were purified using Agencourt AMPure XP beads. For the second PCR, consensus adaptor sequences were added to the 5' end of the target sequence primer using the same PCR parameters except the annealing temperature was 68°C and repeated 22 cycles. For the third PCR, the resulting PCR products from different genes were pooled and then amplified with NEBNext Ultra II DNA library prep kit for Illumina (E7645S, New England Biolabs, Ipswich, MA, USA) using index primers from NEBNext Multiplex Oligos for Illumina (E7335S, New England Biolabs, Ipswich, MA, USA) following manufacturer instructions. The indexed PCR products were cleaned using Agencourt AMPure XP beads and sent for quality control analysis at the University of Minnesota Genomics Center. sTM-seq primers of the target genes were designed using Methyl Primer software v1.0 and the sequences are shown in Table S2. The libraries were sequenced on Mi-Seq in 150 bp paired end mode at the University Minnesota Genomics Center.

Data analysis: To analyze sequencing 150 base reads from MiSeq sequencing of PCR products generated to examine potentially differentially methylated regions were reduced to 90 base per reads using trimmomatic v-33 to remove the first 9 base pairs and base pairs found after position 95 in order to improve mapping efficiency and systematically remove sequencing primer contamination. Samples were mapped to the

mouse genome, or a control sequence containing hydroxy-methylated DNA (for bisulfite and oxBS treatment) using Bismark v 22.3 using HISAT2. Bismark compares mapping to a normal genome as well as a genome where all Cs are reduced. By comparing these mappings where sequence is present, the methylation state of a given sample can be calculated at each C. Methylation percentage at each location was calculated using the bismark_methylation_extractor function to generate files which represent the methylation percentage atC postions within the genome. Files representing methylation frequency at specific locations (.cov) were imported into and analyzed in R.

Competing interests: No competing interests declared.

Funding: This work was funded by grants to T.C.H. from National Institutes of Health (R01CA168622), The Minnesota Masonic Charities, and the Children's Cancer Research Fund, Minneapolis, MN.

Abbreviations

5mC – 5-methylcytosine
5hmC – 5-hydroxymethylcytosine
5fC – 5-formylcytosine
CGI – CpG Island
ESCs - embryonic stem cells
FPKM - Fragments Per Kilobase of transcript per Million mapped reads
GCL - ganglion cell layer
hMeDIP-qPCR - 5hmC-DNA immunoprecipitation followed by quantitative PCR
HPLC – high performance liquid chromatography
INL - inner nuclear layer
NBL - neuroblastic layer
ONL - outer nuclear layer
OPL - outer plexiform layer
oxBS – oxidatative bisulfite

P0 - post-natal day 0

pRB - retinoblastoma protein

qPCR – quantitative PCR

RPC - retinal progenitor cell

RGC – retinal ganglionic cell

SHH - sonic hedgehog

sTM-Seq – simultaneous targeted methylation sequencing

REFERENCES

AGATHOCLEOUS, M. & HARRIS, W. A. 2009. From progenitors to differentiated cells in the vertebrate retina. *Annu Rev Cell Dev Biol,* 25**,** 45-69.

ALDIRI, I., XU, B., WANG, L., CHEN, X., HILER, D., GRIFFITHS, L., VALENTINE, M., SHIRINIFARD, A., THIAGARAJAN, S., SABLAUER, A., BARABAS, M. E., ZHANG, J., JOHNSON, D., FRASE, S., ZHOU, X., EASTON, J., MARDIS, E. R., WILSON, R. K., DOWNING, J. R. & DYER, M. A. 2017. The Dynamic Epigenetic Landscape of the Retina During Development, Reprogramming, and Tumorigenesis. *Neuron,* 94**,** 550-568 e10.

ANGILERI, K. M. & GROSS, J. M. 2020. dnmt1 function is required to maintain retinal stem cells within the ciliary marginal zone of the zebrafish eye. *Sci Rep,* 10**,** 11293.

ASMUS, N., PAPALE, L. A., MADRID, A. & ALISCH, R. S. 2019. Simultaneous Targeted Methylation Sequencing (sTM-Seq). *Curr Protoc Hum Genet,* 101**,** e81.

AUSTIN, C. P., FELDMAN, D. E., IDA, J. A., JR. & CEPKO, C. L. 1995. Vertebrate retinal ganglion cells are selected from competent progenitors by the action of Notch. *Development,* 121**,** 3637-50.

BACHMAN, M., URIBE-LEWIS, S., YANG, X., WILLIAMS, M., MURRELL, A. & BALASUBRAMANIAN, S. 2014. 5-Hydroxymethylcytosine is a predominantly stable DNA modification. *Nat Chem,* 6**,** 1049-55.

BASSETT, E. A. & WALLACE, V. A. 2012. Cell fate determination in the vertebrate retina. *Trends Neurosci,* 35**,** 565-73.

BAYE, L. M. & LINK, B. A. 2007. Interkinetic nuclear migration and the selection of neurogenic cell divisions during vertebrate retinogenesis. *J Neurosci,* 27**,** 10143-52.

BLANCHART, A., NAVIS, A. C., ASSAIFE-LOPES, N., USOSKIN, D., ARANDA, S., SONTHEIMER, J. & ERNFORS, P. 2018. UHRF1 Licensed Self-Renewal of Active Adult Neural Stem Cells. *Stem Cells,* 36**,** 1736-1751.

BOSTICK, M., KIM, J. K., ESTÈVE, P. O., CLARK, A., PRADHAN, S. & JACOBSEN, S. E. 2007. UHRF1 plays a role in maintaining DNA methylation in mammalian cells. *Science,* 317**,** 1760-4.

BRONNER, C., ACHOUR, M., ARIMA, Y., CHATAIGNEAU, T., SAYA, H. & SCHINI-KERTH, V. B. 2007. The UHRF family: oncogenes that are drugable targets for cancer therapy in the near future? *Pharmacol Ther.,* 115**,** 419-34.

BRZEZINSKI, J. A. & REH, T. A. 2015. Photoreceptor cell fate specification in vertebrates. *Development,* 142**,** 3263-73.

BUSTIN, S. A., BENES, V., GARSON, J. A., HELLEMANS, J., HUGGETT, J., KUBISTA, M., MUELLER, R., NOLAN, T., PFAFFL, M. W., SHIPLEY, G. L., VANDESOMPELE, J. & WITTWER, C. T. 2009. The MIQE guidelines: minimum information for publication of quantitative real-time PCR experiments. *Clin Chem,* 55**,** 611-22.

BUSTIN, S. A. & WITTWER, C. T. 2017. MIQE: A Step Toward More Robust and Reproducible Quantitative PCR. *Clin Chem,* 63**,** 1537-1538.

CENTANIN, L. & WITTBRODT, J. 2014. Retinal neurogenesis. *Development,* 141**,** 241-4.

CEPKO, C. 2014. Intrinsically different retinal progenitor cells produce specific types of progeny. *Nat Rev Neurosci,* 15**,** 615-27.

CEPKO, C. L., AUSTIN, C. P., YANG, X., ALEXIADES, M. & EZZEDDINE, D. 1996. Cell fate determination in the vertebrate retina. *Proc Natl Acad Sci U S A,* 93**,** 589-95.

CHEN, R., ZHANG, Q., DUAN, X., YORK, P., CHEN, G. D., YIN, P., ZHU, H., XU, M., CHEN, P., WU, Q., LI, D., SAMARUT, J., XU, G., ZHANG, P., CAO, X., LI, J. & WONG, J. 2017. The 5-hydroxymethylcytosine (5hmC) reader Uhrf2 is required for normal levels of 5hmC in mouse adult brain and spatial learning and memory. *J Biol Chem*.

CHEN, X. R., SUN, S. C., TENG, S. W., LI, L., BIE, Y. F., YU, H., LI, D. L., CHEN, Z. Y. & WANG, Y. 2018. Uhrf2 deletion impairs the formation of hippocampus-dependent memory by changing the structure of the dentate gyrus. *Brain Struct Funct,* 223**,** 609-618.

CLARK, B. S., STEIN-O'BRIEN, G. L., SHIAU, F., CANNON, G. H., DAVIS-MARCISAK, E., SHERMAN, T., SANTIAGO, C. P., HOANG, T. V., RAJAII, F., JAMES-ESPOSITO, R. E., GRONOSTAJSKI, R. M., FERTIG, E. J., GOFF, L. A. & BLACKSHAW, S. 2019. Single-Cell RNA-Seq Analysis of Retinal Development Identifies NFI Factors as Regulating Mitotic Exit and Late-Born Cell Specification. *Neuron,* 102**,** 1111-1126.e5.

CORSO-DÍAZ, X., JAEGER, C., CHAITANKAR, V. & SWAROOP, A. 2018. Epigenetic control of gene regulation during development and disease: A view from the retina. *Prog Retin Eye Res,* 65**,** 1-27.

DEL BENE, F., WEHMAN, A. M., LINK, B. A. & BAIER, H. 2008. Regulation of neurogenesis by interkinetic nuclear migration through an apical-basal notch gradient. *Cell,* 134**,** 1055-65.

DVORIANTCHIKOVA, G., SEEMUNGAL, R. J. & IVANOV, D. 2019. DNA Methylation Dynamics During the Differentiation of Retinal Progenitor Cells Into Retinal Neurons Reveal a Role for the DNA Demethylation Pathway. *Front Mol Neurosci,* 12**,** 182.

DYER, M. A. & CEPKO, C. L. 2001. Regulating proliferation during retinal development. *Nat Rev Neurosci,* 2**,** 333-42.

DYSON, N. J. 2016. RB1: a prototype tumor suppressor and an enigma. *Genes Dev,* 30**,** 1492-502.

FICZ, G., BRANCO, M. R., SEISENBERGER, S., SANTOS, F., KRUEGER, F., HORE, T. A., MARQUES, C. J., ANDREWS, S. & REIK, W. 2011. Dynamic regulation of 5-hydroxymethylcytosine in mouse ES cells and during differentiation. *Nature,* 473**,** 398-402.

FILTZ, E. A., EMERY, A., LU, H., FORSTER, C. L., KARASCH, C. & HALLSTROM, T. C. 2015. Rb1 and Pten Co-Deletion in Osteoblast Precursor Cells Causes Rapid Lipoma Formation in Mice. *PLoS One,* 10**,** e0136729.

HAHN, M. A., QIU, R., WU, X., LI, A. X., ZHANG, H., WANG, J., JUI, J., JIN, S. G., JIANG, Y., PFEIFER, G. P. & LU, Q. 2013. Dynamics of 5-hydroxymethylcytosine and chromatin marks in Mammalian neurogenesis. *Cell Rep,* 3**,** 291-300.

HAHN, M. A., SZABO, P. E. & PFEIFER, G. P. 2014. 5-Hydroxymethylcytosine: a stable or transient DNA modification? *Genomics,* 104**,** 314-23.

HE, B., ZHANG, C., ZHANG, X., FAN, Y., ZENG, H., LIU, J., MENG, H., BAI, D., PENG, J., ZHANG, Q., TAO, W. & YI, C. 2021. Tissue-specific 5-hydroxymethylcytosine landscape of the human genome. *Nat Commun,* 12**,** 4249.

HE, Y. F., LI, B. Z., LI, Z., LIU, P., WANG, Y., TANG, Q., DING, J., JIA, Y., CHEN, Z., LI, L., SUN, Y., LI, X., DAI, Q., SONG, C. X., ZHANG, K., HE, C. & XU, G. L. 2011. Tet-mediated formation of 5-carboxylcytosine and its excision by TDG in mammalian DNA. *Science,* 333**,** 1303-7.

HON, G. C., SONG, C. X., DU, T., JIN, F., SELVARAJ, S., LEE, A. Y., YEN, C. A., YE, Z., MAO, S. Q., WANG, B. A., KUAN, S., EDSALL, L. E., ZHAO, B. S., XU, G. L., HE, C. & REN, B. 2014. 5mC oxidation by Tet2 modulates enhancer activity and timing of transcriptome reprogramming during differentiation. *Mol Cell,* 56**,** 286-97.

ITO, S., SHEN, L., DAI, Q., WU, S. C., COLLINS, L. B., SWENBERG, J. A., HE, C. & ZHANG, Y. 2011. Tet proteins can convert 5-methylcytosine to 5-formylcytosine and 5-carboxylcytosine. *Science,* 333**,** 1300-3.

JEANBLANC, M., MOUSLI, M., HOPFNER, R., BATHAMI, K., MARTINET, N., ABBADY, A. Q., SIFFERT, J. C., MATHIEU, E., MULLER, C. D. & BRONNER, C. 2005. The retinoblastoma gene and its product are targeted by ICBP90: a key mechanism in the G1/S transition during the cell cycle. *Oncogene,* 24**,** 7337-45.

JIA, Y., LI, P., FANG, L., ZHU, H., XU, L., CHENG, H., ZHANG, J., LI, F., FENG, Y., LI, Y., LI, J., WANG, R., DU, J. X., CHEN, T., JI, H., HAN, J., YU, W., WU, Q. & WONG, J. 2016. Negative regulation of DNMT3A de novo DNA methylation by frequently overexpressed UHRF family proteins as a mechanism for widespread DNA hypomethylation in cancer. *Cell Discov,* 2**,** 16007.

KIM, J. W., YANG, H. J., BROOKS, M. J., ZELINGER, L., KARAKÜLAH, G., GOTOH, N., BOLEDA, A., GIESER, L., GIUSTE, F., WHITAKER, D. T., WALTON, A., VILLASMIL, R., BARB, J. J., MUNSON, P. J., KAYA, K. D., CHAITANKAR, V., COGLIATI, T. & SWAROOP, A. 2016. NRL-Regulated Transcriptome Dynamics of Developing Rod Photoreceptors. *Cell Rep,* 17**,** 2460-2473.

KOH, K. P. & RAO, A. 2013. DNA methylation and methylcytosine oxidation in cell fate decisions. *Curr Opin Cell Biol,* 25**,** 152-61.

KRIAUCIONIS, S. & HEINTZ, N. 2009. The nuclear DNA base 5-hydroxymethylcytosine is present in Purkinje neurons and the brain. *Science,* 324**,** 929-30.

LAI, M., LIANG, L., CHEN, J., QIU, N., GE, S., JI, S., SHI, T., ZHEN, B., LIU, M., DING, C., WANG, Y. & QIN, J. 2016. Multidimensional Proteomics Reveals a Role of UHRF2 in the Regulation of Epithelial-Mesenchymal Transition (EMT). *Mol Cell Proteomics,* 15**,** 2263-78.

LI, L., DUAN, Q., ZENG, Z., ZHAO, J., LU, J., SUN, J., ZHANG, J., SIWKO, S., WONG, J., SHI, T., ZHANG, X., LIU, M., CHEN, J. & LI, D. 2020. UHRF2 promotes intestinal tumorigenesis through stabilization of TCF4 mediated Wnt/β-catenin signaling. *Int J Cancer*.

LI, Y., MORI, T., HATA, H., HOMMA, Y. & KOCHI, H. 2004. NIRF induces G1 arrest and associates with Cdk2. *Biochem Biophys Res Commun. ,* 319**,** 464-8.

LIU, X., GAO, Q., LI, P., ZHAO, Q., ZHANG, J., LI, J., KOSEKI, H. & WONG, J. 2013. UHRF1 targets DNMT1 for DNA methylation through cooperative binding of hemi-methylated DNA and methylated H3K9. *Nat Commun,* 4**,** 1563.

LIU, X., XU, B., YANG, J., HE, L., ZHANG, Z., CHENG, X., YU, H., LIU, X., JIN, T., PENG, Y., HUANG, Y., XIA, L., WANG, Y., WU, J., WU, X., LIU, S., SHAN, L., YANG, X., SUN, L., LIANG, J., ZHANG, Y. & SHANG, Y. 2021. UHRF2 commissions the completion of DNA demethylation through allosteric activation by 5hmC and K33-linked ubiquitination of XRCC1. *Mol Cell,* 81**,** 2960-2974.e7.

LIU, Y., ZHANG, B., KUANG, H., KORAKAVI, G., LU, L. Y. & YU, X. 2016. Zinc Finger Protein 618 Regulates the Function of UHRF2 (Ubiquitin-like with PHD and Ring Finger Domains 2) as a Specific 5-Hydroxymethylcytosine Reader. *J Biol Chem,* 291**,** 13679-88.

LIU, Y., ZHANG, B., MENG, X., KORN, M. J., PARENT, J. M., LU, L. Y. & YU, X. 2017. UHRF2 regulates local 5-methylcytosine and suppresses spontaneous seizures. *Epigenetics,* 12**,** 551-560.

LIVAK, K. J. & SCHMITTGEN, T. D. 2001. Analysis of relative gene expression data using real-time quantitative PCR and the 2(-Delta Delta C(T)) Method. *Methods,* 25**,** 402-8.

LIVESEY, F. J. & CEPKO, C. L. 2001. Vertebrate neural cell-fate determination: lessons from the retina. *Nat Rev Neurosci,* 2**,** 109-18.

LU, H., BHOOPATIRAJU, S., WANG, H., SCHMITZ, N. P., WANG, X., FREEMAN, M. J., FORSTER, C. L., VERNERIS, M. R., LINDEN, M. A. & HALLSTROM, T. C. 2016. Loss of UHRF2 expression is associated with human neoplasia, promoter hypermethylation, decreased 5-hydroxymethylcytosine, and high proliferative activity. *Oncotarget*.

LU, H. & HALLSTROM, T. C. 2012. Sensitivity to TOP2 targeting chemotherapeutics is regulated by Oct1 and FILIP1L. *PLoS One,* 7**,** e42921.

LU, H. & HALLSTROM, T. C. 2013. The nuclear protein UHRF2 is a direct target of the transcription factor E2F1 in the induction of apoptosis. *J Biol Chem,* 288**,** 23833-43.

LU, H., LIANG, X., ISSAENKO, O. A. & HALLSTROM, T. C. 2011. Jab1/CSN5 mediates E2F dependent expression of mitotic and apoptotic but not DNA replication targets. *Cell Cycle,* 10**,** 1-10.

LUO, T., CUI, S., BIAN, C. & YU, X. 2013. Uhrf2 is important for DNA damage response in vascular smooth muscle cells. *Biochem Biophys Res Commun,* 441**,** 65-70.

MERBS, S. L., KHAN, M. A., HACKLER, L., JR., OLIVER, V. F., WAN, J., QIAN, J. & ZACK, D. J. 2012. Cell-specific DNA methylation patterns of retina-specific genes. *PLoS One,* 7**,** e32602.

MO, A., LUO, C., DAVIS, F. P., MUKAMEL, E. A., HENRY, G. L., NERY, J. R., URICH, M. A., PICARD, S., LISTER, R., EDDY, S. R., BEER, M. A., ECKER, J. R. & NATHANS, J. 2016. Epigenomic landscapes of retinal rods and cones. *Elife,* 5**,** e11613.

MOOTHA, V. K., LINDGREN, C. M., ERIKSSON, K. F., SUBRAMANIAN, A., SIHAG, S., LEHAR, J., PUIGSERVER, P., CARLSSON, E., RIDDERSTRÅLE, M., LAURILA, E., HOUSTIS, N., DALY, M. J., PATTERSON, N., MESIROV, J. P., GOLUB, T. R., TAMAYO, P., SPIEGELMAN, B., LANDER, E. S., HIRSCHHORN, J. N., ALTSHULER, D. & GROOP, L. C. 2003. PGC-1alpha-responsive genes involved in oxidative phosphorylation are coordinately downregulated in human diabetes. *Nat Genet,* 34**,** 267-73.

MORI, T., IKEDA, D. D., FUKUSHIMA, T., TAKENOSHITA, S. & KOCHI, H. 2011. NIRF constitutes a nodal point in the cell cycle network and is a candidate tumor suppressor. *Cell Cycle,* 10**,** 3284-99.

MORI, T., LI, Y., HATA, H., ONO, K. & KOCHI, H. 2002. NIRF, a novel RING finger protein, is involved in cell-cycle regulation. *Biochem Biophys Res Commun.,* 296**,** 530-6.

MOTNENKO, A., LIANG, C. C., YANG, D., LOPEZ-MARTINEZ, D., YOSHIKAWA, Y., ZHAN, B., WARD, K. E., TIAN, J., HAAS, W., SPINGARDI, P., KESSLER, B. M., KRIAUCIONIS, S., GYGI, S. P. & COHN, M. A. 2018. Identification of UHRF2 as a novel DNA interstrand crosslink sensor protein. *PLoS Genet,* 14**,** e1007643.

MU, X. & KLEIN, W. H. 2004. A gene regulatory hierarchy for retinal ganglion cell specification and differentiation. *Semin Cell Dev Biol,* 15**,** 115-23.

MUNOZ, J., STANGE, D. E., SCHEPERS, A. G., VAN DE WETERING, M., KOO, B. K., ITZKOVITZ, S., VOLCKMANN, R., KUNG, K. S., KOSTER, J., RADULESCU, S., MYANT, K., VERSTEEG, R., SANSOM, O. J., VAN ES, J. H., BARKER, N., VAN OUDENAARDEN, A., MOHAMMED, S., HECK, A. J. & CLEVERS, H. 2012. The Lgr5 intestinal stem cell signature: robust expression of proposed quiescent '+4' cell markers. *Embo j,* 31**,** 3079-91.

NASONKIN, I. O., LAZO, K., HAMBRIGHT, D., BROOKS, M., FARISS, R. & SWAROOP, A. 2011. Distinct nuclear localization patterns of DNA methyltransferases in developing and mature mammalian retina. *J Comp Neurol,* 519**,** 1914-30.

NASONKIN, I. O., MERBS, S. L., LAZO, K., OLIVER, V. F., BROOKS, M., PATEL, K., ENKE, R. A., NELLISSERY, J., JAMRICH, M., LE, Y. Z., BHARTI, K., FARISS, R. N., RACHEL, R. A., ZACK, D. J., RODRIGUEZ-BOULAN, E. J. & SWAROOP, A. 2013. Conditional knockdown of DNA methyltransferase 1 reveals a key role of retinal pigment epithelium integrity in photoreceptor outer segment morphogenesis. *Development,* 140**,** 1330-41.

NEVINS, J. R. 1998. Toward an understanding of the functional complexity of the E2F and Retinoblastoma families. *Cell Growth & Diff.,* 9**,** 585-593.

OHNUMA, S. & HARRIS, W. A. 2003. Neurogenesis and the cell cycle. *Neuron,* 40**,** 199-208.

ONODERA, A., GONZÁLEZ-AVALOS, E., LIO, C. J., GEORGES, R. O., BELLACOSA, A., NAKAYAMA, T. & RAO, A. 2021. Roles of TET and TDG in DNA demethylation in proliferating and non-proliferating immune cells. *Genome Biol,* 22**,** 186.

PERERA, A., EISEN, D., WAGNER, M., LAUBE, S. K., KUNZEL, A. F., KOCH, S., STEINBACHER, J., SCHULZE, E., SPLITH, V., MITTERMEIER, N., MULLER, M., BIEL, M., CARELL, T. & MICHALAKIS, S. 2015. TET3 is recruited by REST for context-specific hydroxymethylation and induction of gene expression. *Cell Rep,* 11**,** 283-94.

PICHLER, G., WOLF, P., SCHMIDT, C. S., MEILINGER, D., SCHNEIDER, K., FRAUER, C., FELLINGER, K., ROTTACH, A. & LEONHARDT, H. 2011. Cooperative DNA and histone binding by Uhrf2 links the two major repressive epigenetic pathways. *J Cell Biochem. ,* 112**,** 2585-93.

RAMESH, V., BAYAM, E., CERNILOGAR, F. M., BONAPACE, I. M., SCHULZE, M., RIEMENSCHNEIDER, M. J., SCHOTTA, G. & GOTZ, M. 2016. Loss of Uhrf1 in neural stem cells leads to activation of retroviral elements and delayed neurodegeneration. *Genes Dev,* 30**,** 2199-2212.

RASMUSSEN, K. D. & HELIN, K. 2016. Role of TET enzymes in DNA methylation, development, and cancer. *Genes Dev,* 30**,** 733-50.

RHEE, K. D., YU, J., ZHAO, C. Y., FAN, G. & YANG, X. J. 2012. Dnmt1-dependent DNA methylation is essential for photoreceptor terminal differentiation and retinal neuron survival. *Cell Death Dis,* 3**,** e427.

ROBERTSON, K. D., AIT-SI-ALI, S., YOKOCHI, T., WADE, P. A., JONES, P. L. & WOLFFE, A. P. 2000. DNMT1 forms a complex with Rb, E2F1 and HDAC1 and represses transcription from E2F-responsive promoters. *Nature Genetics,* 25**,** 338-342.

ROTHBART, S. B., KRAJEWSKI, K., NADY, N., TEMPEL, W., XUE, S., BADEAUX, A. I., BARSYTE-LOVEJOY, D., MARTINEZ, J. Y., BEDFORD, M. T., FUCHS, S. M., ARROWSMITH, C. H. & STRAHL, B. D. 2012. Association of UHRF1 with methylated H3K9 directs the maintenance of DNA methylation. *Nat Struct Mol Biol. ,* 19**,** 1155-60.

ROWAN, S. & CEPKO, C. L. 2004. Genetic analysis of the homeodomain transcription factor Chx10 in the retina using a novel multifunctional BAC transgenic mouse reporter. *Dev Biol.,* 271**,** 388-402.

SARVER, A. L., XIE, C., RIDDLE, M. J., FORSTER, C. L., WANG, X., LU, H., WAGNER, W., TOLAR, J. & HALLSTROM, T. C. 2021. Retinoblastoma tumor cell proliferation is negatively associated with an immune gene expression signature and increased immune cells. *Lab Invest*.

SERITRAKUL, P. & GROSS, J. M. 2014. Expression of the de novo DNA methyltransferases (dnmt3 - dnmt8) during zebrafish lens development. *Dev Dyn,* 243**,** 350-6.

SERITRAKUL, P. & GROSS, J. M. 2017. Tet-mediated DNA hydroxymethylation regulates retinal neurogenesis by modulating cell-extrinsic signaling pathways. *PLoS Genet,* 13**,** e1006987.

SERITRAKUL, P. & GROSS, J. M. 2019. Genetic and epigenetic control of retinal development in zebrafish. *Curr Opin Neurobiol,* 59**,** 120-127.

SHARIF, J., MUTO, M., TAKEBAYASHI, S., SUETAKE, I., IWAMATSU, A., ENDO, T. A., SHINGA, J., MIZUTANI-KOSEKI, Y., TOYODA, T., OKAMURA, K., TAJIMA, S., MITSUYA, K., OKANO, M. & KOSEKI, H. 2007. The SRA protein Np95 mediates epigenetic inheritance by recruiting Dnmt1 to methylated DNA. *Nature,* 450**,** 908-12.

SHEN, L. & ZHANG, Y. 2013. 5-Hydroxymethylcytosine: generation, fate, and genomic distribution. *Curr Opin Cell Biol,* 25**,** 289-96.

SILVA, A. O., ERCOLE, C. E. & MCLOON, S. C. 2003. Regulation of ganglion cell production by Notch signaling during retinal development. *J Neurobiol,* 54**,** 511-24.

SINGH, R. K., MALLELA, R. K., HAYES, A., DUNHAM, N. R., HEDDEN, M. E., ENKE, R. A., FARISS, R. N., STERNBERG, H., WEST, M. D. & NASONKIN, I. O. 2017. Dnmt1, Dnmt3a and Dnmt3b cooperate in photoreceptor and outer plexiform layer development in the mammalian retina. *Exp Eye Res,* 159**,** 132-146.

SPRUIJT, C. G., GNERLICH, F., SMITS, A. H., PFAFFENEDER, T., JANSEN, P. W., BAUER, C., MÜNZEL, M., WAGNER, M., MÜLLER, M., KHAN, F., EBERL, H. C., MENSINGA, A., BRINKMAN, A. B., LEPHIKOV, K., MÜLLER, U., WALTER, J., BOELENS, R., VAN INGEN, H., LEONHARDT, H., CARELL, T. & VERMEULEN, M. 2013 Dynamic readers for 5-(hydroxy)methylcytosine and its oxidized derivatives. *Cell,* 152**,** 1146-59.

SUBRAMANIAN, A., TAMAYO, P., MOOTHA, V. K., MUKHERJEE, S., EBERT, B. L., GILLETTE, M. A., PAULOVICH, A., POMEROY, S. L., GOLUB, T. R., LANDER, E. S. & MESIROV, J. P. 2005. Gene set enrichment analysis: a knowledge-based approach for interpreting genome-wide expression profiles. *Proc Natl Acad Sci U S A,* 102**,** 15545-50.

SWAROOP, A., KIM, D. & FORREST, D. 2010. Transcriptional regulation of photoreceptor development and homeostasis in the mammalian retina. *Nat Rev Neurosci,* 11**,** 563-76.

TAHILIANI, M., KOH, K. P., SHEN, Y., PASTOR, W. A., BANDUKWALA, H., BRUDNO, Y., AGARWAL, S., IYER, L. M., LIU, D. R., ARAVIND, L. & RAO, A. 2009. Conversion of 5-methylcytosine to 5-hydroxymethylcytosine in mammalian DNA by MLL partner TET1. *Science,* 324**,** 930-5.

VANDENBOSCH, L. S. & REH, T. A. 2020. Epigenetics in neuronal regeneration. *Semin Cell Dev Biol,* 97**,** 63-73.

VAUGHAN, R. M., DICKSON, B. M., CORNETT, E. M., HARRISON, J. S., KUHLMAN, B. & ROTHBART, S. B. 2018. Comparative biochemical analysis of UHRF proteins reveals molecular mechanisms that uncouple UHRF2 from DNA methylation maintenance. *Nucleic Acids Res,* 46**,** 4405-4416.

WAID, D. K. & MCLOON, S. C. 1995. Immediate differentiation of ganglion cells following mitosis in the developing retina. *Neuron,* 14**,** 117-24.

WALLACE, V. A. 2011. Concise review: making a retina--from the building blocks to clinical applications. *Stem Cells,* 29**,** 412-7.

WANG, Y., DAKUBO, G. D., THURIG, S., MAZEROLLE, C. J. & WALLACE, V. A. 2005. Retinal ganglion cell-derived sonic hedgehog locally controls proliferation and the timing of RGC development in the embryonic mouse retina. *Development,* 132**,** 5103-13.

WEBER, A. R., KRAWCZYK, C., ROBERTSON, A. B., KUŚNIERCZYK, A., VÅGBØ, C. B., SCHUERMANN, D., KLUNGLAND, A. & SCHÄR, P. 2016. Biochemical reconstitution of TET1-TDG-BER-dependent active DNA demethylation reveals a highly coordinated mechanism. *Nat Commun,* 7**,** 10806.

WEINBERG, R. A. 1995. The retinoblastoma protein and cell cycle control. *Cell,* 81**,** 323-330.

XIANG, M. 2013. Intrinsic control of mammalian retinogenesis. *Cell Mol Life Sci,* 70**,** 2519-32.

XIE, C., FREEMAN, M. J., LU, H., WANG, X., FORSTER, C. L., SARVER, A. L. & HALLSTROM, T. C. 2017. Retinoblastoma cells activate the AKT pathway and are vulnerable to the PI3K/mTOR inhibitor NVP-BEZ235. *Oncotarget*.

XIE, C., LU, H., NOMURA, A., HANSE, E. A., FORSTER, C. L., PARKER, J. B., LINDEN, M. A., KARASCH, C. & HALLSTROM, T. C. 2015. Co-deleting Pten with Rb in retinal progenitor cells in mice results in fully penetrant bilateral retinoblastomas. *Mol Cancer,* 14**,** 93.

XU, Y., XU, C., KATO, A., TEMPEL, W., ABREU, J. G., BIAN, C., HU, Y., HU, D., ZHAO, B., CEROVINA, T., DIAO, J., WU, F., HE, H. H., CUI, Q., CLARK, E., MA, C., BARBARA, A., VEENSTRA, G. J., XU, G., KAISER, U. B., LIU, X. S., SUGRUE, S. P., HE, X., MIN, J., KATO, Y. & SHI, Y. G. 2012. Tet3 CXXC domain and dioxygenase activity cooperatively regulate key genes for Xenopus eye and neural development. *Cell,* 151**,** 1200-13.

YOUNG, R. W. 1985. Cell proliferation during postnatal development of the retina in the mouse. *Brain Res,* 353**,** 229-39.

YUE, X., TRIFARI, S., ÄIJÖ, T., TSAGARATOU, A., PASTOR, W. A., ZEPEDA-MARTÍNEZ, J. A., LIO, C. W., LI, X., HUANG, Y., VIJAYANAND, P., LÄHDESMÄKI, H. & RAO, A. 2016. Control of Foxp3 stability through modulation of TET activity. *J Exp Med,* 213**,** 377-97.

ZHANG, J., GAO, Q., LI, P., LIU, X., JIA, Y., WU, W., LI, J., DONG, S., KOSEKI, H. & WONG, J. 2011. S phase-dependent interaction with DNMT1 dictates the role of UHRF1 but not UHRF2 in DNA methylation maintenance. *Cell Res.,* 21**,** 1723-39.

ZHANG, J., GRAY, J., WU, L., LEONE, G., ROWAN, S., CEPKO, C. L., ZHU, X., CRAFT, C. M. & DYER, M. A. 2004. Rb regulates proliferation and rod photoreceptor development in the mouse retina. *Nat Genet. ,* 36**,** 351-360.

ZHOU, T., XIONG, J., WANG, M., YANG, N., WONG, J., ZHU, B. & XU, R. M. 2014. Structural basis for hydroxymethylcytosine recognition by the SRA domain of UHRF2. *Mol Cell,* 54**,** 879-86.

Figures

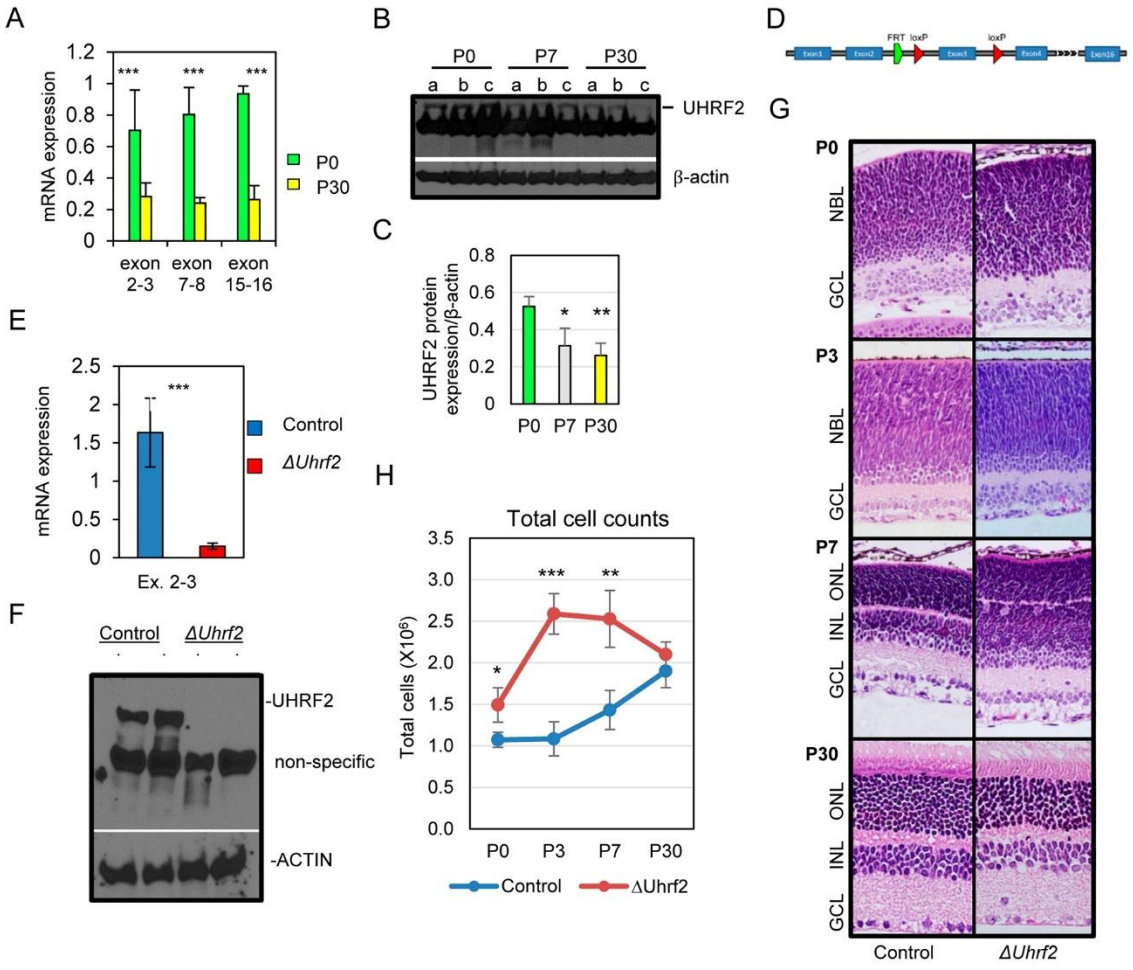

Figure 1. UHRF2 is highly expressed in RPCs and restricts their overproduction. A. RNA was isolated from control retinae from postnatal day 0 (P0) (green) and P30 (yellow) mice for qPCR analysis with primers spanning exons 2-3, 7-8, and 15-16 in *Uhrf2*. B. UHRF2 protein levels were detected at P0, P7, and P30 by immunoblotting with three isolates from independent retinae, with β–actin as loading control. C. Protein bands in (B) were quantified, and UHRF2 protein levels are shown relative to β–actin. P-value comparisons are to P0. D. Schematic of the genomic architecture of the *Uhrf2* gene with *loxP* sites surrounding exon three facilitating conditional deletion. E. Uhrf2-specific deletion from RPCs was achieved by crossing to *Vsx2-Cre:GFP*$^{+}$ line. RNA was isolated from control and *Vsx2-Cre:GFP*$^{+}$*; Uhrf2*$^{fl/fl}$ mice, and primers located within

exons 2 and 3 were used for qPCR analysis to compare and demonstrate loss of *Uhrf2* mRNA from the knockout. F. Retinae from control and *Uhrf2*–deficient mice were harvested and immunoblotted with anti-UHRF2 or anti-actin antisera. Dots indicate two independent replicates for each genotype. G. Representative histological sections from P0, P3, P7 and P30 aged control and *Uhrf2*-deficient retinae stained with hematoxylin & eosin. H. Total retinal cell counts from (G) were quantified by counting 5 retinae from P0, P3, and P7 and P30 control and *Uhrf2*-deficient mice. P-values were determined by two-tailed Student's *t*-test with $p < 0.05$ considered significant. Error bars represent standard deviation from the mean. (NBL, neuroblastic layer; GCL, ganglionic cell layer; ONL, outer nuclear layer; INL, inner nuclear layer; *, p-value < 0.05; **, p-value < 0.01; ***; p-value < 0.001).

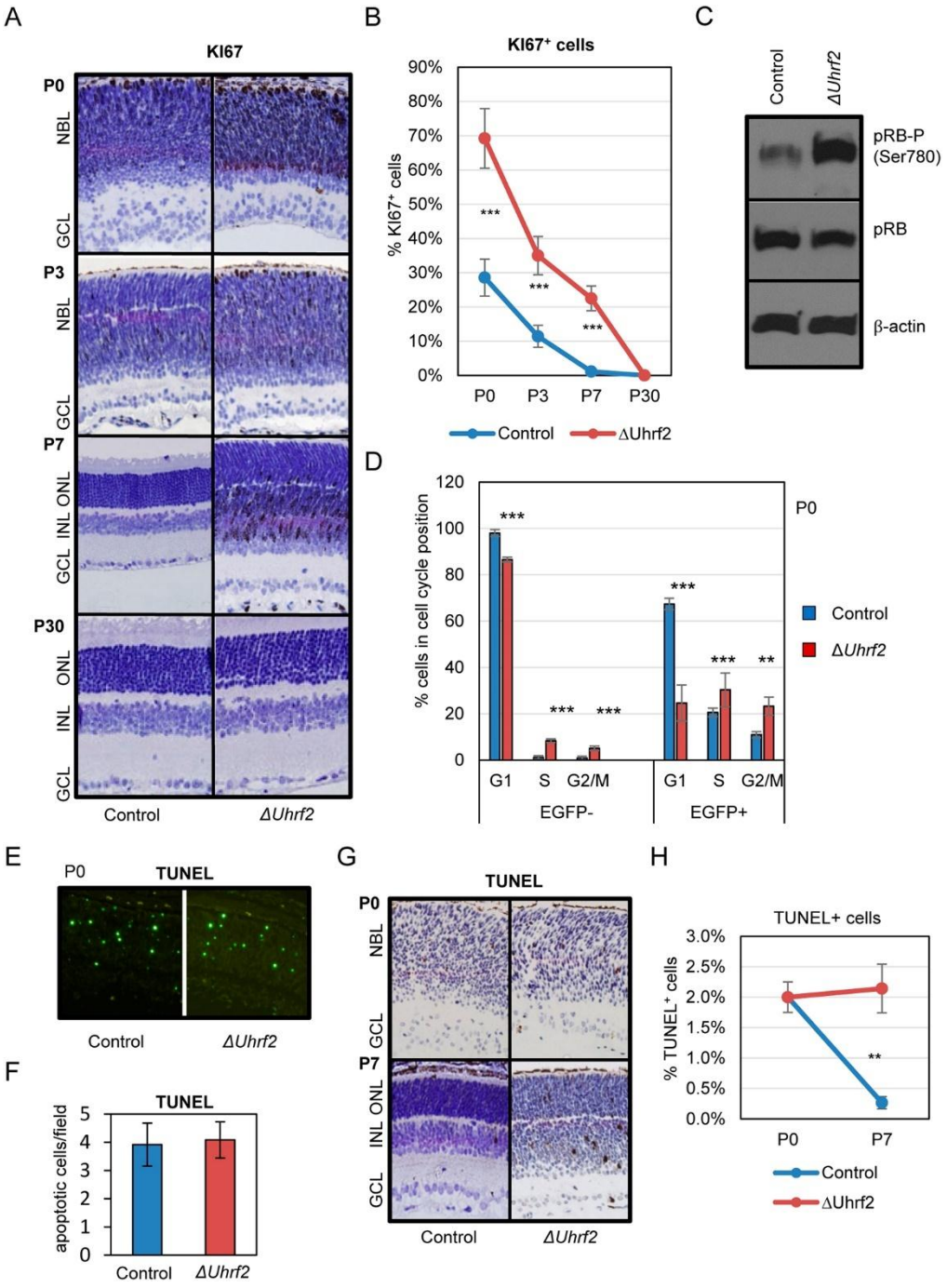

Figure 2. *Uhrf2* deletion causes excess G1/S passage and KI67$^+$ proliferation of retinal progenitor cells. A. KI67$^+$ proliferative cells were detected by immunohistochemistry from wild-type and *Uhrf2*-deficient retinae aged P0, P3, P7, and P30. B. The percent of KI67$^+$ cells from (A) were quantified by counting 5 fields each from three independent control and *Uhrf2*-deficient retinae. C. Protein isolated from P7

control and *Uhrf2*-deficient retinae was immunoblotted with antisera that recognizes retinoblastoma protein phosphorylated at serine 780 (pRB-P), unphosphorylated pRB (pRB), and β–actin as an internal control. D. CRE:EGFP^{-} and CRE:EGFP^{+} retinal cells from control and *Uhrf2*-deficient retinae were isolated from P0 mice and assessed for cell cycle stages by flow cytometry. E. TUNEL^{+} apoptotic cells were detected by immunofluorescence in P0 control and *Uhrf2*-deficient retinae. F. TUNEL^{+} cells from immunofluorescence (E) were quantified by counting 10 fields sized 400μM^{2} from control and *Uhrf2*-deficient retinae (n=3) and graphed and were not significantly different. G. TUNEL^{+} apoptotic cells were detected by immunohistochemistry (IHC) in P0 and P7 control and *Uhrf2*-deficient retinae. H. TUNEL^{+} cells from (G) were quantified by counting 10 fields sized 400μM^{2} from control and *Uhrf2*-deficient retinae (n=3) and graphed. P-values were determined by two-tailed Student's *t*-test with $p < 0.05$ considered significant. Error bars represent standard deviation from the mean. (**, p-value < 0.01; ***; p-value < 0.001).

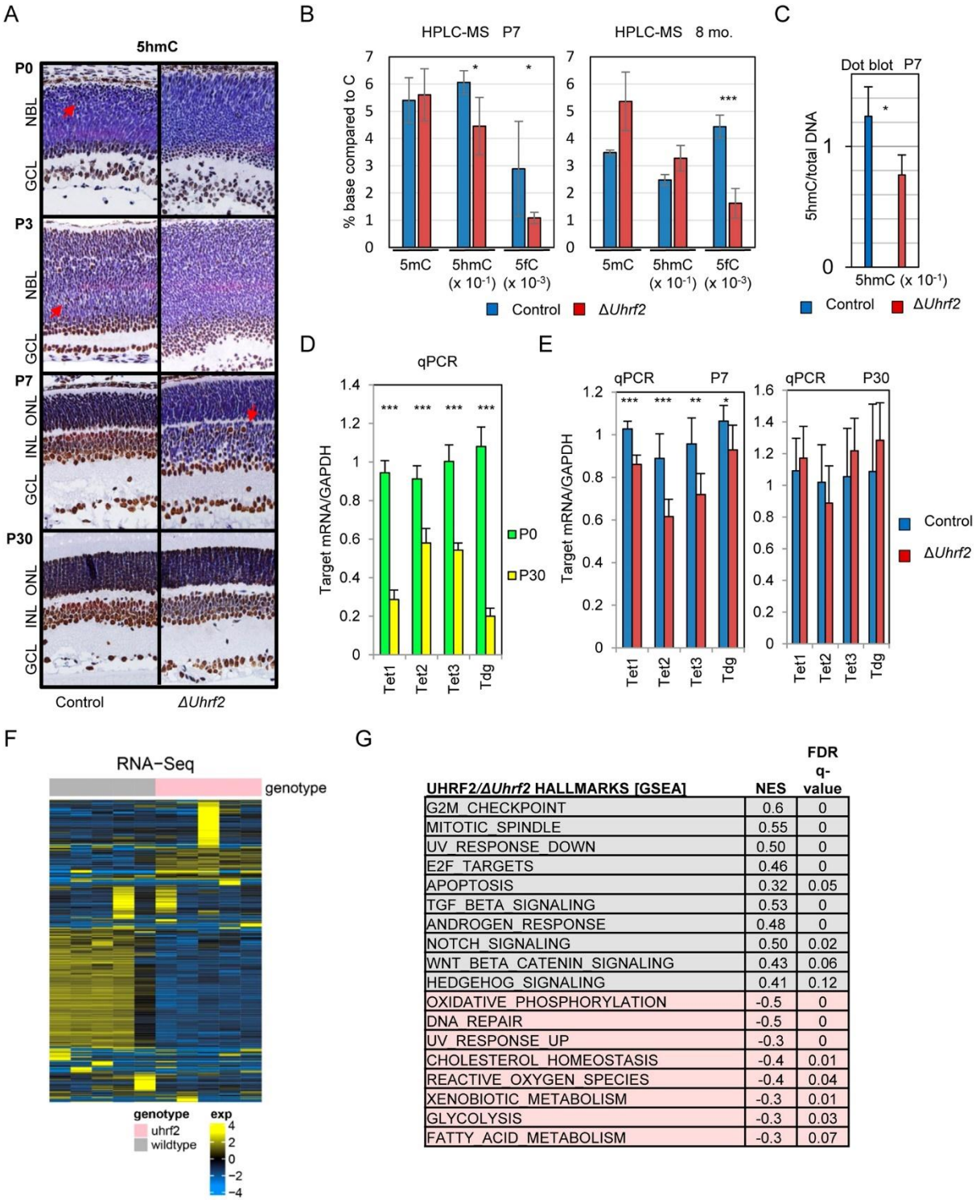

UHRF2/*ΔUhrf2* HALLMARKS [GSEA]	NES	FDR q-value
G2M_CHECKPOINT	0.6	0
MITOTIC_SPINDLE	0.55	0
UV_RESPONSE_DOWN	0.50	0
E2F_TARGETS	0.46	0
APOPTOSIS	0.32	0.05
TGF_BETA_SIGNALING	0.53	0
ANDROGEN_RESPONSE	0.48	0
NOTCH_SIGNALING	0.50	0.02
WNT_BETA_CATENIN_SIGNALING	0.43	0.06
HEDGEHOG_SIGNALING	0.41	0.12
OXIDATIVE_PHOSPHORYLATION	-0.5	0
DNA_REPAIR	-0.5	0
UV_RESPONSE_UP	-0.3	0
CHOLESTEROL_HOMEOSTASIS	-0.4	0.01
REACTIVE_OXYGEN_SPECIES	-0.4	0.04
XENOBIOTIC_METABOLISM	-0.3	0.01
GLYCOLYSIS	-0.3	0.03
FATTY_ACID_METABOLISM	-0.3	0.07

Figure 3. UHRF2 is required for proper 5hmC accumulation and gene expression in the developing retina. A. 5hmC was detected by IHC in retinae of control and *Uhrf2*-deficient retinae at ages P0, P3, P7, and P30. B. Genomic DNA was isolated from P7 (left) and 8-month old (right) control and *Uhrf2*-deficient retinae for HPLC followed by

mass spectrometry to quantify 5mC, 5hmC, and 5-formylcytosine (5fC) levels. C. Genomic DNA from P7 retinae of control and *Uhrf2*-deficient mice was isolated, spotted on nitrocellulose, 5hmC detected with anti-5hmC antisera and quantified against methylene blue total DNA staining. D. RNA was isolated from P0 (green) and P30 (yellow) control retinae for qPCR analysis to determine relative levels of *Tet1*, *Tet2*, *Tet3*, and *Tdg* mRNAs. E. RNA was isolated from control (blue) and *Uhrf2*-deficient (red) retinae at P7 (left) and P30 (right) for qPCR analysis to uncover transcriptional changes to the *Tet1*, *Tet2*, *Tet3*, and *Tdg* genes. F. RNA was isolated from P7 control (wildtype) and *Uhrf2*-deficient (uhrf2) retinae for RNA sequencing analysis. Gene transcripts were ordered by hierarchical clustering and relative transcript expression level is denoted by the color code blue (low) to yellow (high). G. Gene set enrichment analysis (GSEA) comparison of gene expression in control versus *Uhrf2*-deficient retinae at P7 identify genes with reduced (gray) and induced (pink) expression in *Uhrf2*-deficient compared to control retinae. P-values were determined by two-tailed Student's *t*-test with $p < 0.05$ considered significant. Error bars represent standard deviation from the mean. (NES, normalized enrichment score; FDR, false discovery rate; *, p-value < 0.05; **, p-value < 0.01; ***, p-value < 0.001)

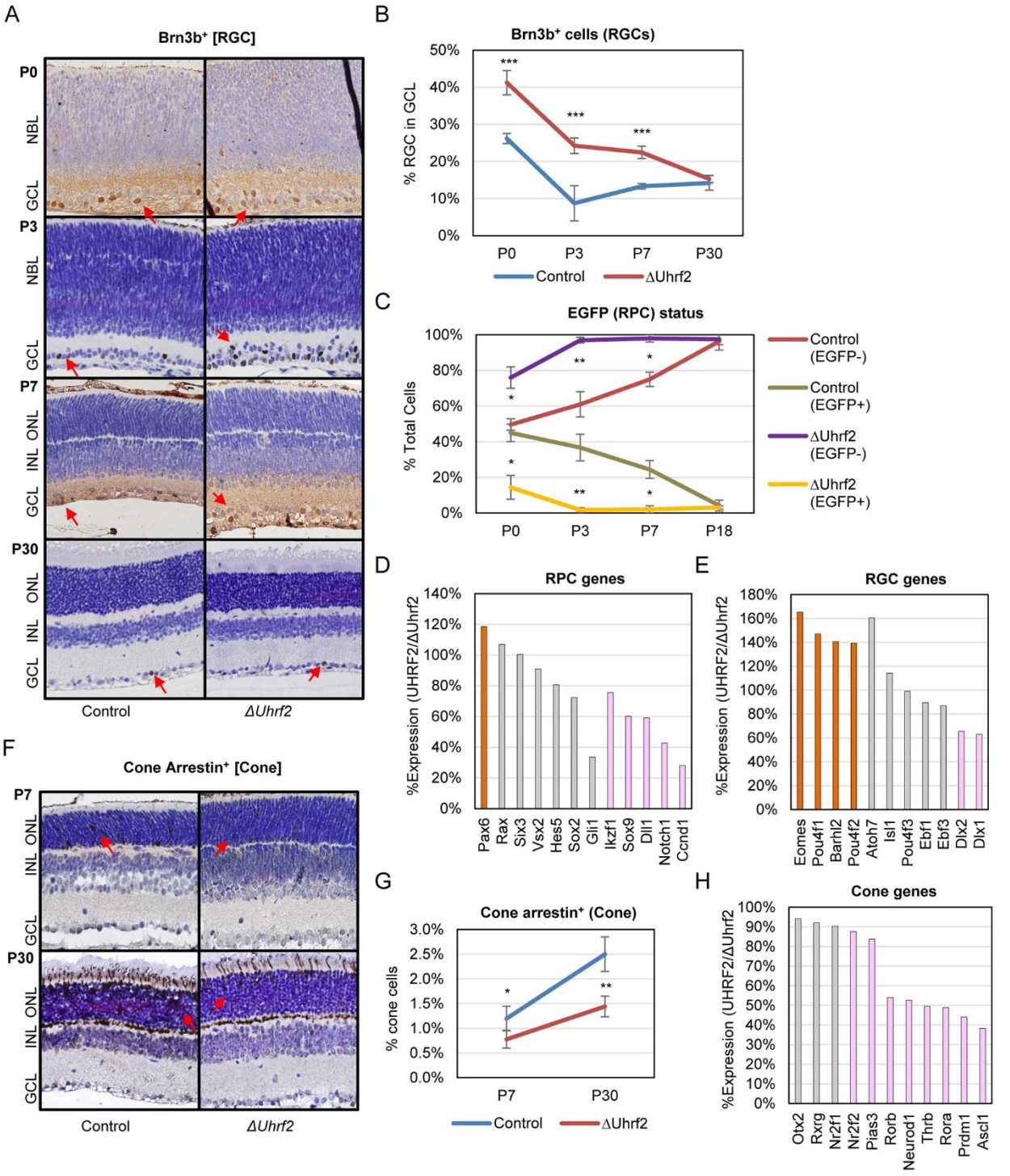

Figure 4. *Uhrf2*-deficiency overproduces retinal ganglion cells (RGC) but reduces retinal progenitor cells (RPC) and cone photoreceptors.

A. RGCs were detected in retinae from P0, P3, P7 or P30 control and *Uhrf2*-deficient mice by IHC with anti-Brn3b antisera (red arrows). B. RGC numbers were quantified and graphed. Numbers are representative of five fields counted from three

independently stained retinae and displayed as %RGCs in the ganglionic cell layer (GCL). C. Numbers of RPCs (EGFP:Cre^{+}) and non-RPCs (EGFP:Cre^{-}) in control and *Uhrf2*-deficient retinae was quantified by flow cytometry at P0, P3, P7, and P18. Color bars designate genotype and EGFP:Cre status. D. Expression levels of RPC genes by RNA-sequencing from P7 retinae. E. Expression levels of RGC genes. F. Cone cells were detected by IHC using anti-cone arrestin antisera on P7 and P30 aged control and *Uhrf2*-deficient retinae (red arrows). G. Cone numbers were quantified and graphed. Numbers are representative of three independently stained retinae and are displayed as per cent cone cells compared to total retinal cells. H. Expression levels of cone genes. For gene expression in (D), (E) and (H), the value is the ratio between expression in *Uhrf2*-deficient vs. control cells. Genes with orange bars are significantly induced and pink bars are significantly reduced. Gray bars represent genes that were not significantly altered. P-values were determined by two-tailed Student's *t*-test with $p < 0.05$ considered significant. Error bars represent standard deviation from the mean. (*, p-value < 0.05; **, p-value < 0.01; ***; p-value < 0.001).

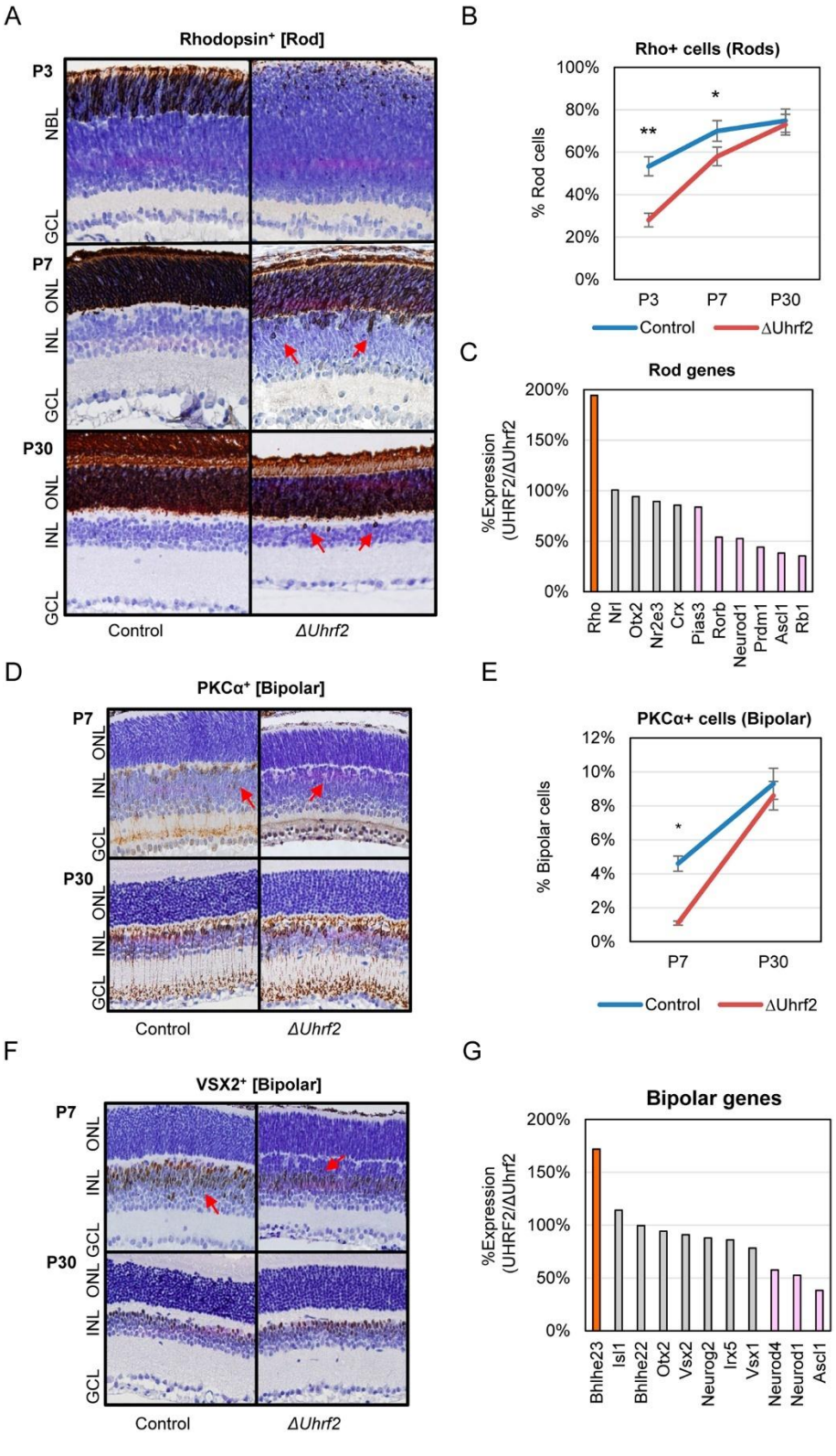

Figure 5. *Uhrf2*-deficiency causes rod cell mislocalization, rhodoposin overproduction, and bipolar cell defects. A. Rod photoreceptor cells were detected by IHC with anti-rhodopsin antibodies in control and *Uhrf2*-deficient retinae at P3, P7, and P30. Red arrows identify rhodopsin^{+} cells that located abnormally in the inner nuclear layer (INL) rather than the outer nuclear layer (ONL). B. The numbers of rod cells from (A) were quantified and graphed. Numbers are representative of five fields from four independently stained retinae and are displayed as percent rod cells compared to total retinal cells. C. Expression levels of rod genes by RNA-sequencing from P7 retinae. D. Bipolar cells were detected by IHC with anti-PKCα antisera in *Uhrf2*-deficient and control retinae at P7 and P30. E. PKCα^{+} staining bipolar cells were quantified and graphed. Numbers are representative of five fields counted from three independently stained retinae and are displayed as percent bipolar cells. F. VSX2^{+} bipolar cells were detected by IHC with anti-VSX2 antisera in *Uhrf2*-deficient and control retinae at P7 and P30. G. Expression levels of bipolar genes by RNA-sequencing from P7 retinae. For gene expression in (C) and (G), the value is the ratio between expressions in *Uhrf2*-deficient vs. control cells. Genes with orange bars are significantly induced and pink bars are significantly reduced. Gray bars represent genes that were not significantly altered. P-values were determined by two-tailed Student's *t*-test with $p < 0.05$ considered significant. Error bars represent standard deviation from the mean. (*, p-value < 0.05; **, p-value < 0.01).

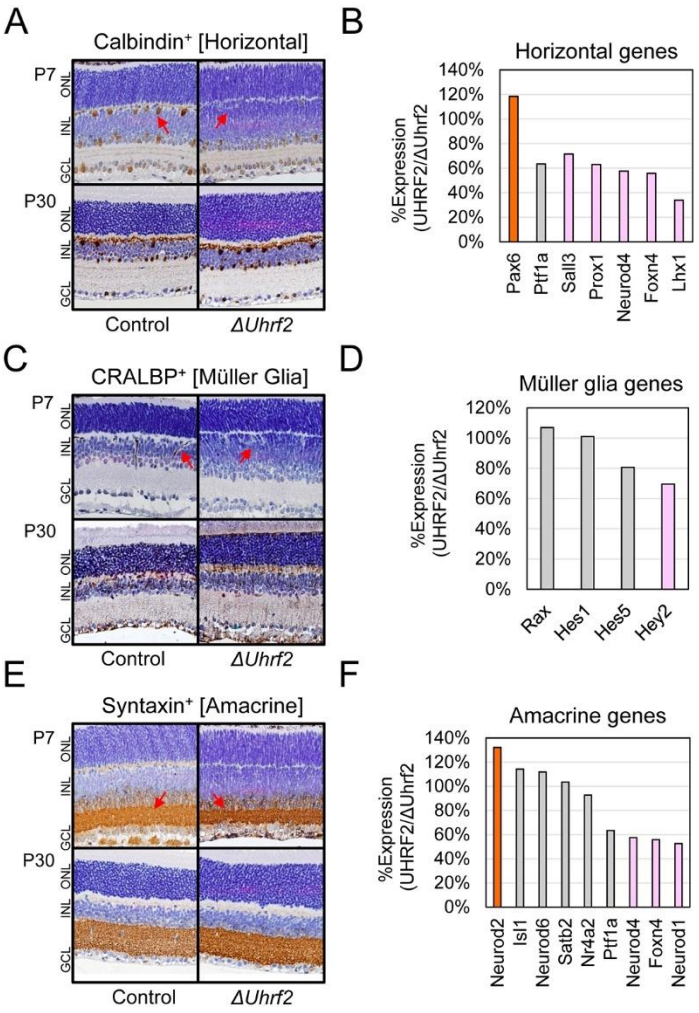

Figure 6. *Uhrf2*-deficiency in retinae causes horizontal and Müller glial cell differentiation defects but doesn't affect amacrine cell production. A. Horizontal cells were detected with anti-calbindin antisera by IHC in P7 and P30 aged control and *Uhrf2*-deficient retinae. B. Expression levels of horizontal cell-promoting genes by RNA-sequencing from P7 retinae. C. Müller glia cells were detected with anti-CRALBP antisera by IHC in P7 and P30 aged control and *Uhrf2*-deficient retinae. D. Expression levels of Müller glia-promoting genes. E. Amacrine cells were detected with anti-Syntaxin antisera by IHC in P7 and P30 aged control and *Uhrf2*-deficient retinae. F. Expression levels of amacrine-promoting genes. For gene expression in (B), (D), and (F), the value is the ratio between expression in *Uhrf2*-deficient vs. control cells. Genes

with orange bars are significantly induced and pink bars are significantly reduced. Gray bars represent genes that were not significantly altered.

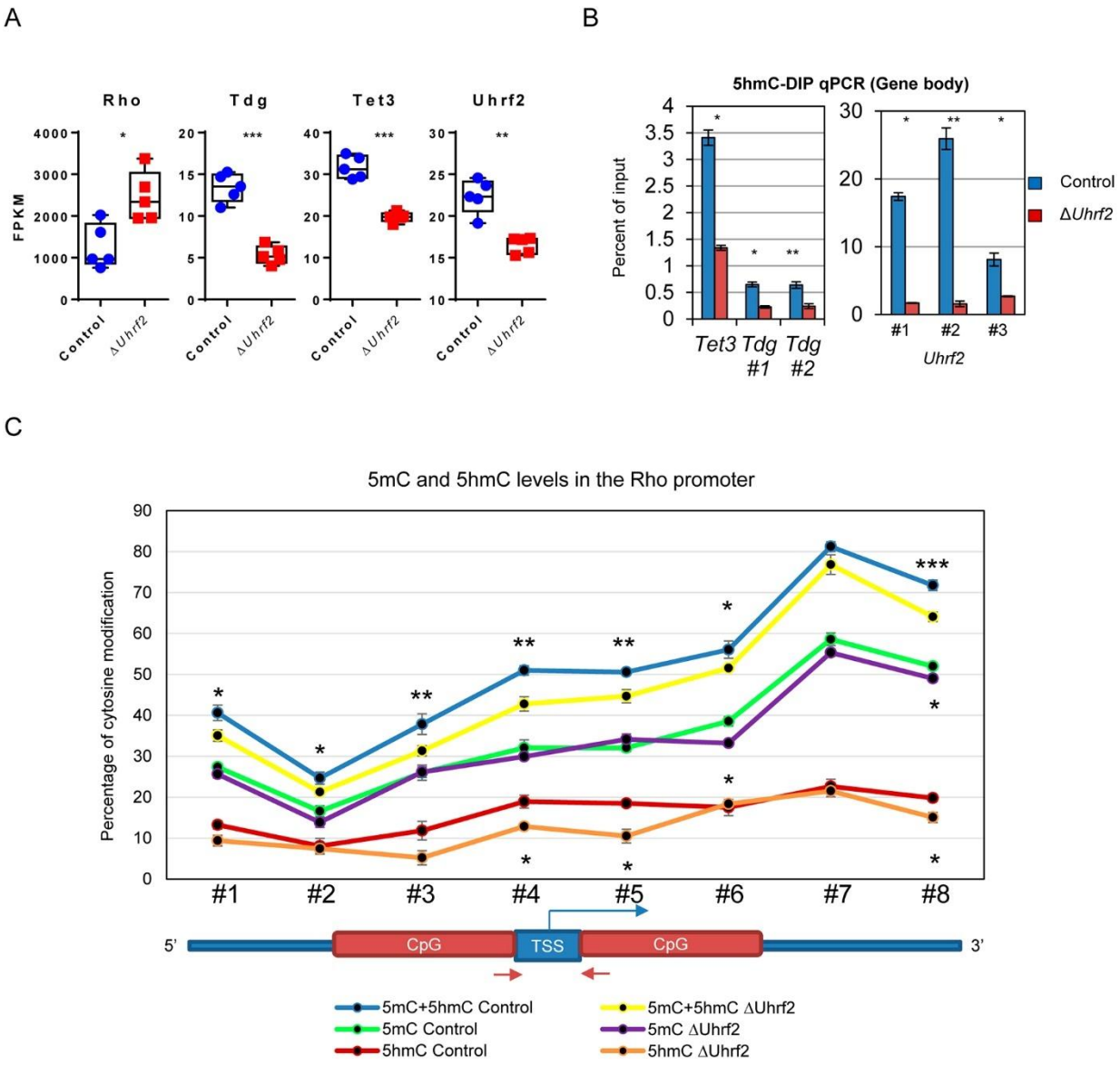

Figure 7. *Uhrf2*-deficiency alters 5mC/5hmC deposition and transcriptional expression of genes involved with active demethylation. A. RNA-sequencing results from P7 control (blue) and *Uhrf2*-deficient (red) retinae to uncover transcriptional changes to the *Rho*, *Tdg*, *Tet3*, and *Uhrf2* genes. B. Genomic DNA was isolated from P7 control and *Uhrf2*-deficient retinae for 5hmC-DNA immunoprecipitation followed by quantitative PCR (hMeDIP-qPCR). Primers locate within the gene body of *Tet3, Tdg* (two primer sets), and *Uhrf2* (three primer sets). C. Genomic DNA was isolated from P7 control and *Uhrf2*-deficient retinae, subjected to both bisulfite (to detect 5mC & 5hmC) and oxidative bisulfite (to detect 5mC) for targeted methylation sequencing (sTM-Seq)

of CpG elements in the *Rho* promoter. 5hmC levels were determined by subtracting the difference between these numbers at each position. P-values were determined by two-tailed Student's *t*-test with $p < 0.05$ considered significant. Error bars represent standard deviation from the mean. (*, p-value < 0.05; **, p-value < 0.01; ***, p-value < 0.001).

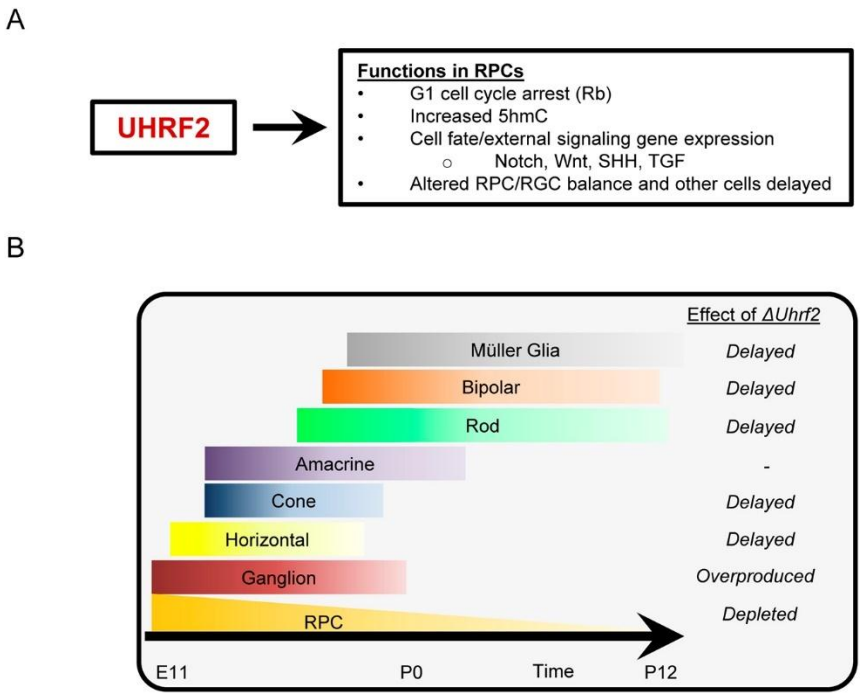

Figure 8. Model describing the activity of UHRF2 in RPCs and effect of *Uhrf2*-deletion on retinal cell differentiation. A. UHRF2 promotes cell cycle arrest in G_1, increases 5hmC, regulates gene expression related to cell cycle and extrinsic signaling, and favors RPC retention over RGC production during retinal development. B. Retinal development in the mouse is affected by *Uhrf2*-deficiency. Shown are the 7 retinal cells types and RPCs, their relative abundance across the mouse retinal developmental time course, and the effect of *Uhrf2* conditional knockout on the characteristics of their development.

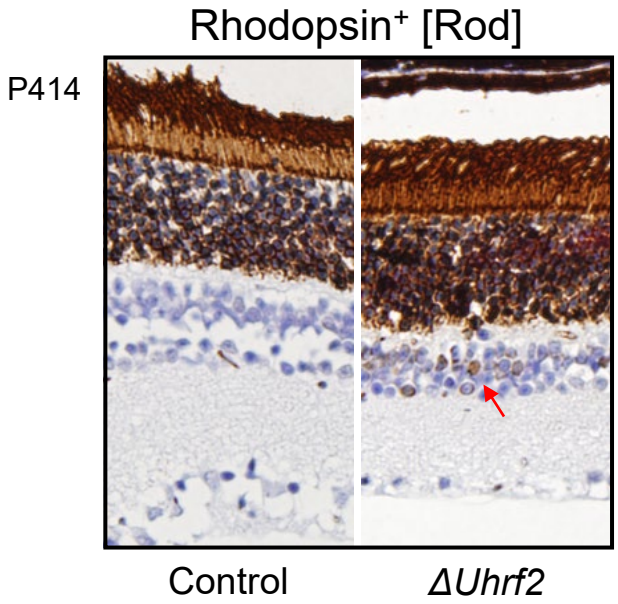

Fig. S1. A. Rod photoreceptor cells were detected by IHC with anti-rhodopsin antibodies in control and *Uhrf*2-deficient retinae at P414.

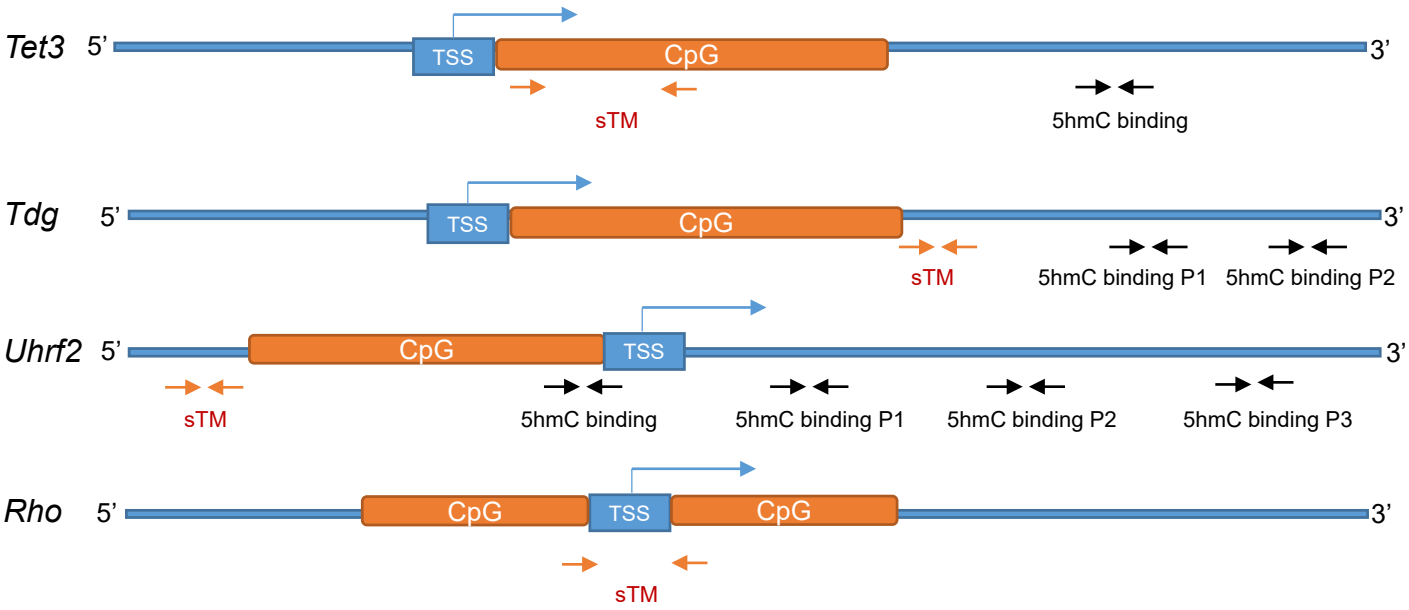

Red: sTM primer position; Black: 5hmC binding Primer position.

Fig. S2. Diagram of the four genes analyzed for 5mC and 5hmC, and the primer locations within them.

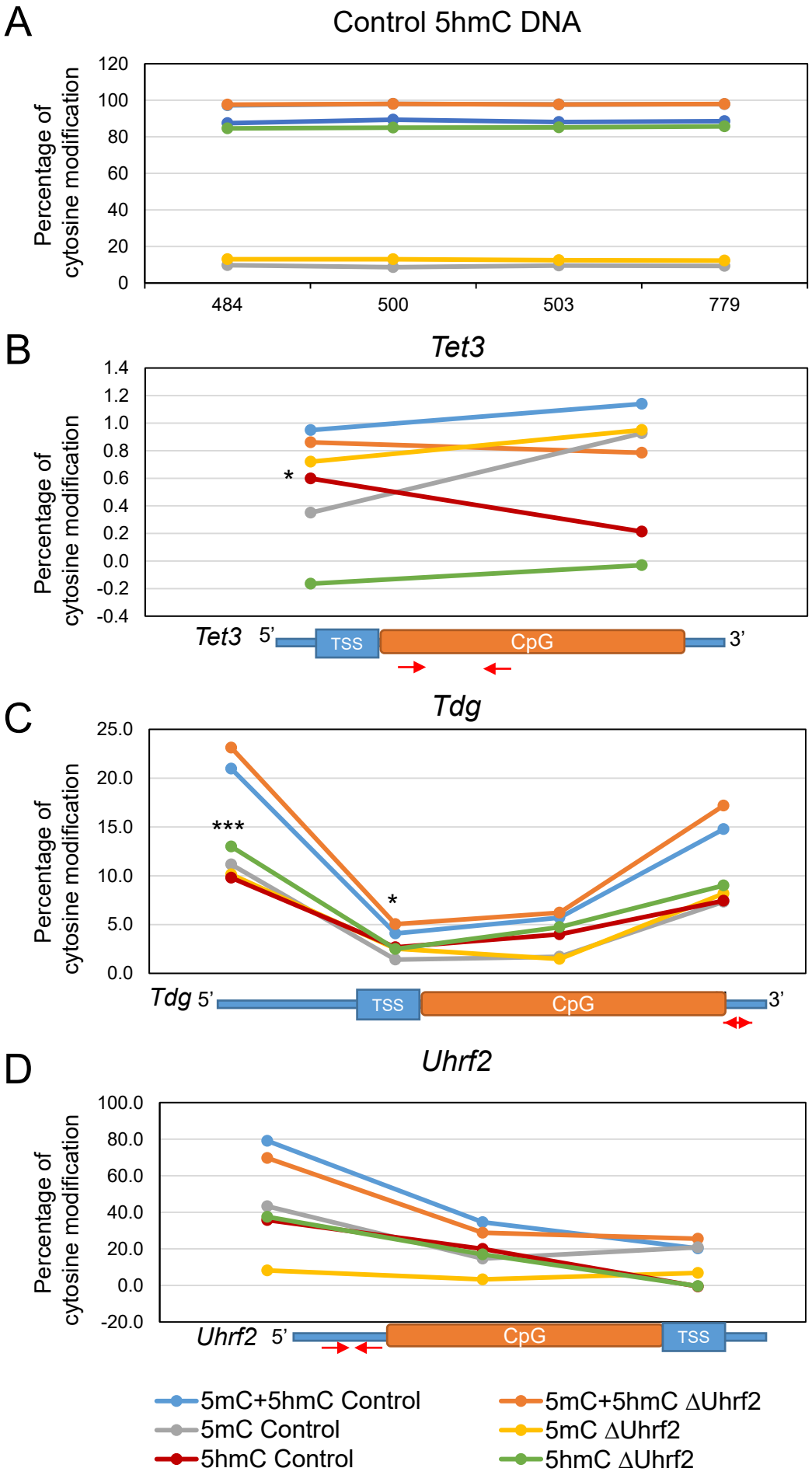

Figure S3.

sTM-Seq analysis, including bisulfite and oxidative-bisulfite conversion, of a 5hmC containing oligonucleotide standard and the *Tet3*, *Uhrf2*, and *Tdg* genes.

Table S1. Mouse primers for qPCR, 5hmC DIP-qPCR, and sTM-Seq

qPCR primers		
Gene	Forward Primer sequence	Reverse primer sequence
Uhrf2 exon 2-3	5'-TTCAGCTGCTAGTTCGTCCA-3'	5'-TTCAAACCAAGCACCAAG GC-3'
Uhrf2 exon 7-8	5'-GTGAGGTGGTAAAGGCTGGA-3'	5'-AACAGGAATACCAGGGATTGG-3'
Uhrf2 exon 15-16	5'-GTGTGTGTGCTGCCAAGAAC-3'	5'-GCAGAGTTTGGAGGGTCTCA-3'
Tet1	5'-TCTCGGGTTAAGGTTGATGC-3'	5'-CCTTTTCGTGTGTCCCTTGT-3'
Tet2	5'-TGAGATGCGGTACTCTGCAC-3'	5'-GTTCTCAACGAGCAGGAAGG-3'
Tet3	5'-TCCGGATTGAGAAGGTCATC-3'	5'-CCAGGCCAGGATCAAGATAA-3'
TdG	5'-GCCAGATGTGCTCAGTTTCC-3'	5'-ACAGCCATCTTCTTTGCGTC-3'
GAPDH	5'-CGTCCCGTAGACAAAATGGT-3'	5'-GAATTTGCCGTGAGTGGAGT-3'
5hmC-DNA immunoprecipitation qPCR primers		
Gene position	Forward primer sequence	Reverse primer sequence
Uhrf2 CpG island	5'-CCATGGCTCCTTCCTATTTG-3'	5'-GCGAGGACTGACGCTCTTAG -3'
Uhrf2 position 1	5'-CCTGAACTTGCCATGTAGAGC-3'	5'-TCTAGCAGGACATGGTGGTG-3'
Uhrf2 position 2	5'-AAACCAGCCTGAGCTGTGTC-3'	5'-TCCGTCTCTGCCTCTCTCTC-3'
Uhrf2 position 3	5'-TGCTGAAGGCATCAGATTCA-3'	5'-CATCCCACAGCTTCTGGTTC-3'
Tet1	5'-TGTGTGTGTGTGTGTTTGTGTG-3'	5'-GACAGGGGCTACATGGAGAA-3'
Tet3	5'-GCCTGACTACACGGCTAACG-3'	5'-GTGTCTGCAGCAGGTCAGTC-3'
TdG position 1	5'-CCAGGCTGGCTTGAACTTAG-3'	5'-AAGGCCACATGTCTTTAATCC-3'
TdG position 2	5'-GTGTTGGGGATGGAACGTAG-3'	5'-CCATGATGGGAGGTAGCAGT-3'
sTM-Seq primers for first round PCR		
Gene	Forward primer	Reverse primer
Tet3	5'-GGAGGTAGTTGGAGTAGGAAG-3'	5'-AAAAAACAAAACAATCCAACAC-3'
TdG	5'-GTTTGTTTTTAAGTGGTAAATGGA-3'	5'-TTTCAACTCCCATAAACTACCA-3'
Uhrf2	5'-TTTTATGGGAATGATTAGTATTGATAT-3'	5'-CCCATCCAAAAATAAAAAACT-3'
Rho	5'-GGTTTAGGGAGAGAAGGTTATTT-3'	5'-AAACACATAAAAATTAAAACCCTCT-3'
5hmC	5'-TGATAAAAGAGTTTGA-3'	5'-ACATTAACCTATAAAAATA-3'
sTM-Seq primers for second round PCR		
Tet3	5'ACACTCTTTCCCTACACGACGCTCTTCCGATCTG GAGGTAGTTGGAGTAGGAAG -3'	5'-GTGACTGGAGTTCAGACGTGTGCTGTTC CGATCTAAAAAACAAAACAATCCAACAC-3'
TdG	5'-ACACTCTTTCCCTACACGACGCTCTTCC GATCTGTTTGTTTTTAAGTGGTAAATGGA-3'	5'-GTGACTGGAGTTCAGACGTGTGCTGTTC CGATCTTTTCAACTCCCATAAACTACCA-3'
Uhrf2	5'-ACACTCTTTCCCTACACGACGCTCTTCCG ATCTTTTTATGGGAATGATTAGTATTGATAT-3'	5'-GTGACTGGAGTTCAGACGTGTGCTGTTC CGATCTCCCATCCAAAAATAAAAAACT-3'
Rho	5-'ACACTCTTTCCCTACACGACGCTCTTCC GATCTGGTTTAGGGAGAGAAGGTTATTT-3'	5'GTGACTGGAGTTCAGACGTGTGCTGTTCC GATCTAAACACATAAAAATTAAAACCCTCT-3'
sTM-Seq adapters for third round PCR		
Tet3	5-'AATGATACGGCGACCACCGAGATCTACACT CTTTCCCTACACGACGCTCTTCCGATC-s-T-3'	5'-CAAGCAGAAGACGGCATACGAGATCGTGAT GTGACTGGAGTTCAGACGTGTGCTCTTCCGATC-s-T-3'
TdG	5'-AATGATACGGCGACCACCGAGATCTACACT CTTTCCCTACACGACGCTCTTCCGATC-s-T-3'	Same, except the index may change
Uhrf2	5-'AATGATACGGCGACCACCGAGATCTACACT CTTTCCCTACACGACGCTCTTCCGATC-s-T-3'	Same, except the index may change
Rho	5'-AATGATACGGCGACCACCGAGATCTACACT CTTTCCCTACACGACGCTCTTCCGATC-s-T-3'	Same, except the index may change

Table S2. List of antibodies used in this study

Antibody		Company	Dilution	Cat#
Ki67		Biocare	(1:50)	CRM325
UHRF2 (C-10)		Santa Cruz Biotechnology	(1:1000)	sc-398953
5hmC		Active Motif	(1:8000 IHC; 1:1000 Dot blot)	39791
Brn3b (C-13)		Santa Cruz Biotechnology	(1:200)	sc-6026
PKC		Sigma	(1:2000)	P5704
Syntaxin		Sigma	(1:8000)	S0664
Calbindin		Sigma	(1:500)	C9848
Rhodopsin 4D2		Novus Biologicals	(1:500)	NBP2-59690
VSX2		Exalpha Biologicals	(1:250)	x1180p
CRALBP		Abcam	(1:200)	ab15051
Cone Arrestin		EMD Millipore	(1:2500)	AB15282
TUNEL (ApopTag)		EMD Millipore	per. Manu.	S7100
Rb-P (Ser780)		Cell Signaling Technology	(1:1000)	8180S
β-actin polyclonal		Sigma	(1:2500)	A2066